Mapping of Mycobacterial Enzymes Involved in Triacylglycerol Accumulation as Intrabacterial Lipid Inclusions Using Activity-Based Multitarget Inhibitor Probes

Romain Avellan, Jordan Lehoux, Thomas Francis, Tonia Dargham, Léa Celik, Alexandre Guy, Isabelle Poncin, Vanessa Point, Laurent Kremer, Thierry Durand, et al.

Mapping of mycobacterial enzymes involved in triacylglycerol accumulation as intrabacterial lipid inclusions using activity-based multi-target inhibitor probes

Romain Avellan[1,#], Jordan Lehoux[2,#], Thomas Francis[1,#], Tonia Dargham[1,3,#], Léa Celik[1], Alexandre Guy[2], Isabelle Poncin[1], Vanessa Point[1], Laurent Kremer[4,5], Thierry Durand[2], Stéphane Audebert[6], Luc Camoin[6], Christopher Spilling[7], Pierre Santucci[1], Céline Crauste[2], Stéphane Canaan[1], Jean-François Cavalier[1]*

[1] Aix-Marseille Univ., CNRS, LISM UMR7255, IMM FR3479, 31 Chemin Joseph Aiguier, 13009 Marseille, France

[2] IBMM, Univ Montpellier, CNRS, ENSCM, 1919 route de Mende, 34293 Montpellier, France Montpellier, France

[3] IHU Méditerranée Infection, Aix-Marseille Univ., 19-21 Boulevard Jean Moulin, 13005 Marseille, France

[4] Centre National de la Recherche Scientifique UMR 9004, Institut de Recherche en Infectiologie de Montpellier (IRIM), Université de Montpellier, 1919 route de Mende, 34293 Montpellier, France

[5] INSERM, IRIM, 34293 Montpellier, France

[6] INSERM, CNRS, Institut Paoli-Calmettes, CRCM, Marseille Protéomique, Aix-Marseille Univ., 27 Boulevard Lei Roure, 13009 Marseille, France

[7] Department of Chemistry and Biochemistry, University of Missouri-St. Louis, 1 University Boulevard, St. Louis, Missouri 63121, United States

[#] These authors contributed equally to this work, and should be considered as first co-authors

[*] Corresponding author: Jean-François Cavalier (jfcavalier@imm.cnrs.fr).

ABSTRACT

Lipids play a critical role in the physiology, life cycle and pathogenicity of mycobacteria. They largely participate in host-pathogen interactions and fulfill important functions ranging from cell wall biosynthesis/maintenance, bacterial growth dynamics and long-term persistence. In that context, triacylglycerol, a specific subtype of neutral lipid is stored as intrabacterial lipid inclusions (ILI), which have been described as important structures for long-term survival and persistence within the host. However, the enzymes involved in ILI formation and degradation remain largely undefined. Using bio-orthogonal click-chemistry activity-based protein profiling (CC-ABPP) of newly synthetized Oxadiazolone (**OX**), Cyclophostin and Cyclipostins (**CyC**) probes, we report the direct capture of target proteins in *Mycobacterium abscessus* growing under carbon excess and nitrogen-deprived *in vitro* conditions that promote triacylglycerol production and ILI formation. This approach led to the identification of a set of 65 enzymes, potentially involved in global processes related to ILI anabolism. Among these, the long-chain-fatty-acid--CoA ligase MAB_1978c/FadD15 has been validated as a pivotal enzyme that colocalizes on ILI and as a major contributor in ILI formation in *M. abscessus*.

KEYWORDS

Activity-based protein profiling; multitarget inhibitor-like activity-based probes; lipid metabolism; Cyclipostins and Cyclophostin; Oxadiazolone; *Mycobacterium abscessus*.

Mycobacteria are known for their unique and complex cell wall architecture,[1] characterized by distinct lipid-rich outer layers, making lipid metabolism a central point of their physiological processes. One crucial aspect of mycobacteria relies in their ability to metabolize host lipids and to accumulate the resulting neutral lipids in their own cytoplasm in the form of intrabacterial lipid inclusions (ILI).[2-3] These lipid-rich organelles consist of a hydrophobic core containing neutral lipids, essentially triacylglycerol (TAG), surrounded by a phospholipid monolayer, associated with numerous proteins.[4] These ILI serve as reservoirs for energy storage and provide also a platform for the synthesis and maintenance of lipids, which are essential for the adaptability and survival of mycobacteria under various stresses.[2,5-6] This is particularly true in the case of Mycobacterium tuberculosis, the causative agent of tuberculosis (TB), where ILI play a critical role in pathogenesis and contribute to the establishment and maintenance of the infection process.[5] In addition, ILI increase tolerance to first-line anti-TB drugs.[7]

ILI have been reported in all mycobacterial species;[8] including pathogenic (*i.e.*, *Mycobacterium leprae*,[9] *Mycobacterium canettii*[10], *M. tuberculosis*,[4-5,11] *Mycobacterium abscessus*,[12-13] *Mycobacterium avium*,[6] *Mycobacterium marinum*,[14] and *Mycobacterium ulcerans*[15]) as well as saprophytic mycobacteria (*i.e.*, *M. smegmatis*[12,16]); suggesting a conserved function of these organelles in the mycobacterial lifecycle and physiology.[8] Among them, *M. abscessus* also referred to as an "antibiotic and clinical nightmare"[17-18] is one of the most drug-resistant mycobacterial species.[19] It causes pulmonary diseases in immunocompromised and vulnerable individuals, including cystic fibrosis (CF) and bronchiectasis patients.[20] *M. abscessus* exists as two distinct colony morphotypes, a smooth (S) and rough (R), associated with different clinical outcomes.[19-20] While the S morphotype is more hydrophilic, with increased sliding motility and biofilm formation, the R variant has a high propensity to produce large bacterial serpentine cords.[20] In fact, the S variant is viewed as the environmental and colonizing form, while the R variant has been proposed to emerge during the infection process, and is frequently associated with severe pulmonary infections[21] especially in infected CF patients.[22] Finally, due to its intrinsic polyresistance to a wide range of

antibiotics,[18] including most anti-TB agents, *M. abscessus* has become a major public health concern with a significant economic burden associated with poorly effective treatments. Like *M. tuberculosis*, *M. abscessus* accumulates TAG under the form of ILI, a phenotype associated with an enhanced pathogenesis and antibiotic tolerance,[12-13] suggesting that ILI metabolism constitutes an important aspect in the physiopathology of pathogenic mycobacteria.

How mycobacteria acquire host lipids and how ILI are formed remain, however, largely unanswered questions. While these issues have been tackled, mostly by studying pure recombinant lipolytic enzymes secreted by mycobacteria,[11,13,23-24] studies dedicated to the identification and characterization of proteins involved in ILI accumulation and consumption remain scarce.[4,16]

Stimulated by these observations, we developed two robust experimental models to report ILI formation and degradation, to mimic lipid metabolism during the non-replicating and regrowth stages.[25] The first model is based on infected murine bone-marrow-derived macrophages (mBMDM) fed with Very Low-Density Lipoproteins (VLDL) to trigger the differentiation of the macrophages into foamy macrophages.[6,11] In this specific environment, mycobacteria are able to accumulate host lipids to form ILI, and further hydrolyze these stored ILI upon removal of VLDL from the culture medium, thus mimicking bacterial regrowth and reactivation of the disease. The second one is an *in vitro* and reversible model based on carbon excess and nitrogen starvation allowing *in vitro* ILI biosynthesis and hydrolysis in living *M. abscessus*.[12]

Interestingly, using these two models, we demonstrated that the presence of hydrolase inhibitors impaired TAG accumulation in the form of ILI as well as their further hydrolysis,[11-12] confirming the involvement of mycobacterial lipid synthesizing and hydrolyzing enzymes in the ILI accumulation and consumption processes. Most enzymes participating in ILI metabolism are members of the hydrolase family, mainly distributed among serine- and cysteine-hydrolases that possess a catalytic serine or cysteine residue (*i.e.*, (Ser/Cys)-based enzymes). This family includes esterases, dienelactone hydrolases, epoxide hydrolases, haloalkane dehalogenases, lipases, thioesterases, and peptidases.[26-27]

Our group has previously reported the antimycobacterial activity of two families of enzyme inhibitors, namely the Oxadiazolone compounds (**OX**) and the Cyclophostin & Cyclipostins analogs (**CyC**), both of which exhibit potent inhibitory activity against mycobacterial (Ser/Cys)-based enzymes by forming a covalent bond with their respective catalytic serine or cysteine residue.[23,28-29] Non-toxic to murine macrophages (CC_{50}>100 µM), both **OX** and **CyC** efficiently inhibit the growth of *M. tuberculosis* and *M. abscessus* in broth medium and/or within infected macrophages.[23,30-35]

To identify the putative mycobacterial target enzyme(s) of the best **OX** and **CyC** growth inhibitors, activity-based protein profiling (ABPP) approach[27,36-43] was employed. Using competitive ABPP, the comparative proteomic analysis between the control sample (*i.e.*, DMSO) and the *M. tuberculosis*[32-33] and *M. abscessus*[30,32] cell culture pre-treated with the best **OX** (*i.e.*, **iB*p*PPOX** or **HPOX**) or **CyC** (*i.e.*, **CyC$_{17}$**) prior to ActivX^{TM} Desthiobiotin-FP probe labeling resulted in mass spectrometry identification of the target proteins of each inhibitor. Most of the identified proteins are (Ser/Cys)-based enzymes related to global lipid metabolism (cholesterol and free fatty acid) and cell wall biosynthesis. Among them, the bifunctional thioesterase-phospholipase LipG,[44] the mycolyltransferase Ag85C,[30,45] the thioesterase TesA,[46] and the carbon-carbon hydrolase HsaD[47] have been validated as effective targets. Notably, we confirmed these results by resolving the crystal structures of Ag85C, TesA and HsaD in complex with a **CyC** inhibitor.[45-47] Consequently, the use of these multi-target inhibitors as efficient activity-based probes (ABP) to decipher the metabolic pathways used by the mycobacteria to catabolize host-derived lipids (cholesterol and fatty acids), notably by identifying key enzymes involved in the accumulation and consumption of ILI, will provide valuable data related to cellular and molecular mechanisms crucial for mycobacteria survival, persistence and virulence.[2]

In the present study, we report the synthesis and use of two **OX** and **CyC** ABPs bearing either a terminal alkyne function or a fluorescent tag to decipher ILI formation in *M. abscessus* using the nitrogen-deprived (MSM-NL)[12] *in vitro* model. By capitalizing from two structurally distinct classes of alkyne-containing inhibitors, the Oxadiazolone-core and the monocyclic enolphosphate derivatives

that display strong complementarity in terms of reactivity and enzymatic affinity,[23] we have captured a broad spectrum of (Ser/Cys)-based target enzymes involved in these lipidic processes *via* bio-orthogonal click-chemistry ABPP (CC-ABPP).[27,36-37,39-40,42-43,48] Among the proteins identified, the long-chain-fatty-acid--CoA ligase MAB_1978c/FadD15 has been validated as a key enzyme that colocalizes on the ILI and contributes to their formation in *M. abscessus*.

RESULTS AND DISCUSSION

Rationale for the design and synthesis of CyC and OX activity-based probes.

Despite all the results generated from previous studies related to the identification of **OX**[30,32] and **CyC**[31,33] target enzymes from *M. tuberculosis* and *M. abscessus* cultures or total lysates, the main disadvantage of competitive ABPP lies in the fact that this approach is mostly an indirect identification that measures the reduction in the probe-labeling signals to assess inhibitor targets.

To overcome this limitation, we have recently reported the synthesis of two efficient **CyC** ABPs[35,47] (**Figure 1A**). First, the **CyC** core-structure was modified by the direct introduction of a Dansyl fluorescent moiety (*i.e.*, **CyC$_{31\text{-Dansyl}}$**[35]). The **CyC$_{\text{-Dansyl}}$** probe was successfully employed to label live mycobacteria through the covalent binding of the **CyC$_{31\text{-Dansyl}}$** to (Ser/Cys)-based enzymes.[35] As a result, the **CyC** penetration inside *M. abscessus* cells was monitored and quantified based on the fluorescent signal, thus validating this **CyC$_{\text{-Dansyl}}$** as an efficient probe.[35] In parallel, we reported the synthesis of a **CyC** derivative containing a terminal alkyne function (*i.e.*, **CyC$_{31\text{yne}}$**), and described its use for the direct capture of target proteins in *M. tuberculosis* cultures by direct CC-ABPP approach.[47] We confirmed the multi-target nature of the **CyC$_{\text{yne}}$** probe and underscored also its use as an effective ABP to unravel metabolic pathways by which *M. tuberculosis* and other mycobacterial species, catabolize lipids to ensure their survival and growth.

Regarding the **OX** molecules, based on our previous work on *M. abscessus*[30] and *M. tuberculosis*,[32] the **HPOX** derivative, which exhibited moderate antibacterial activity (MIC_{50} ~ 45-93 µM[30,32]) against the two species, was selected for chemical structure modification by addition of either a

fluorescent NBD tag (*i.e.*, **HP-NBD-OX**) or a terminal alkyne group (*i.e.*, **HPOX$_{yne}$**) (**Figure 1A** and **Scheme 1**). The NBD fluorophore was chosen mainly because of its small size, which allows convenient coupling to the aromatic ring of **HPOX,** and because of its widespread use for fluorescent labeling of enzyme inhibitors and its tolerance to microorganisms.[49] Its incorporation on the aromatic phenyl ring of the **HPOX** chemical structure was achieved in three consecutive steps with introduction of the fluorescent NBD group after oxadiazolone ring formation (**Scheme 1A**). The synthesis started from commercial *p*-nitrophenyl hydrazine (**1**) that was engaged into the one-pot two-steps cyclisation process in presence of hexyl chloroformate (**2**). Catalytic hydrogenation of the nitro-oxadiazolone (**3**) over palladium led to the aniline derivative (**4**), which was further coupled through a nucleophilic substitution using NBD-chloride to afford the desired fluorescent **HP-NBD-OX** in 13% overall yields. The new **HPOX$_{yne}$** click-ready derivative was further synthesized in a one-pot two-steps reaction using the methodology reported earlier to access the **HPOX** compound[32] (**Scheme 1B**). Briefly, commercially available phenylhydrazine hydrochloride (**5**) and hexyne chloroformate (**6**) formed *in situ* from 5-hexyn-1-ol (**7**) were used in basic conditions to produce a carbamate intermediate (*step i*) that was directly involved in the cyclization reaction in presence of diphosgene (*step ii*) to generate the desired **HPOX$_{yne}$** derivative in 47% yields.[32,50]

Finally, the **CyC$_{31yne}$** and **CyC$_{31\text{-}Dansyl}$** activity-based probes, as well as the corresponding **CyC$_{31}$** parental molecule, were synthesized as previously described.[35,47]

The CyC and OX activity-based probes retain antibacterial activity comparable to their parental molecules. The antimicrobial potency of the selected **CyC** probes [**CyC$_{31yne}$** and **CyC$_{31\text{-}Dansyl}$**] as well as the **OX** ABPs [**HPOX$_{yne}$** and **HP-NBD-OX**] was next evaluated against the S and R variants of *M. abscessus* and compared to that of their parental molecules, *i.e.*, **CyC$_{31}$** and **HPOX**, respectively. The minimal inhibitory concentrations (MIC) leading to 50% and 90% bacterial growth inhibition (*i.e.*, MIC_{50} / MIC_{90}) were determined by the resazurin microtiter assay (REMA) and are reported in **Figure 1B**.[30-31,35,51] Importantly, **HPOX$_{yne}$** and **HP-NBD-OX**, retained the same

moderate antibacterial activity as the unmarked parental **HPOX** molecule, with fold changes in MIC_{50} / MIC_{90} ranging from ×0.7-1.0 / ×1.3-2.0. We previously reported[35] that **CyC$_{31\text{-Dansyl}}$** exhibited extracellular activity comparable to the parent unlabeled **CyC$_{31}$** compound, with very good (MIC_{50} = 1.4 µM / MIC_{90} = 6.1 µM) to moderate (MIC_{50} = 24.1 µM / MIC_{90} = 63.4 µM) anti-mycobacterial activity against *M. abscessus* S and R, respectively (**Figure 1B**). In addition, and as expected from our previous work on *M. tuberculosis*,[47] **CyC$_{31yne}$** showed similar antibacterial activities against *M. abscessus* S (MIC_{50} = 0.84 µM / MIC_{90} = 2.1 µM) and R (MIC_{50} = 10.3 µM / MIC_{90} = 18.5 µM) variants compared to unmodified **CyC$_{31}$**, with a fold change in MICs of ×0.7 to ×1.75 (**Figure 1B**). Overall, these results indicate that incorporation of a fluorescent group or an alkyne bond at the position tested does not alter the activity of the **OX** & **CyC** activity-based probes. In addition to determining their MICs values, a prerequisite for using these ABPs to identify mycobacterial enzymes involved in ILI accumulation was to verify their ability to ***i)*** spatially colocalize with ILI structures and ***ii)*** limit the total TAG content in *M. abscessus* grown in nitrogen-limited MSM-NL.

Fluorescent OX and CyC activity-based probes spatially colocalize with ILI structures inside *M. abscessus*. To confirm the colocalization of **OX** & **CyC** ABPs with ILI inside lipid-rich bacteria, *M. abscessus* S was grown in MSM or MSM-NL for 24 h, harvested and resuspended in fresh medium in the presence of each fluorescent probe at a 100 µM final concentration for an additional 24 h. The **HP$_{\text{-NBD}}$-OX-** and **CyC$_{31\text{-Dansyl}}$**-treated bacteria were stained with Nile Red for ILI labeling[12] and processed for fluorescent microscopy. As expected,[12] *M. abscessus* cultured in MSM-NL medium harbored clear, intense and compact cytoplasmic signal in the form of foci due to ILI staining. In both cases, a clear colocalization of the Dansyl and NBD fluorescent signal with Nile Red ILI-positive areas was observed (**Figure 1C**). Subsequent statistical analysis of the data applying the Coloc2 plugin of ImageJ/Fiji, allowed calculation of the colocalization parameters: the Manders and Pearson coefficients, and the intensity correlation quotient (ICQ) value as suggested by Li.[52] Manders' coefficients which estimate the co-occurrence fraction of a fluorescent signal on one channel (*i.e.*, red

color) with a fluorescent signal of another channel (*i.e.*, green color), vary from 0 (non-overlapping images) to 1 (100% colocalization between two images). Pearson's coefficient evaluate the correlation between two signals and ranges from -1 to 1, with 1 standing for complete positive correlation and -1 for a negative one, while a 0 value indicates no correlation.[53] The statistical significance of these computed correlation coefficients has been assessed by the Costes randomization test,[54] resulting in a Costes' *p*-value which should be ≥95%. Finally, the ICQ value varies from 0.5 (colocalization) to -0.5 (exclusion). Here, colocalization analyses resulted in Pearson's correlation coefficients and Manders' colocalization coefficients[53] (overlap of green and red pixels) of 0.788-0.808 and 0.845-1, respectively; together with a Costes *p*-value[54] of 1, and Li's ICQ value[52] of 0.280-0.324, supporting colocalization (see **Supporting Information** for parameters' full detail).

In contrast, when cells were grown in MSM, the absence of ILI resulted in only low and mainly peripheral Nile Red staining corresponding to cell wall-associated lipids labeling (**Figure S1**). Consequently, as previously reported in the case of labeled **CyC$_{\text{-Dansyl}}$**-mycobacteria,[35] the diffuse fluorescence (*i.e.*, pale green and orange resulting colors) observed with the **HP$_{\text{-NBD}}$-OX** & **CyC$_{\text{31-Dansyl}}$**-treated *M. abscessus* grown in MSM is likely to result from a homogeneous distribution of the probes in the cell wall and/or the cytoplasm of the bacteria.

ILI accumulation is partially blocked by (Ser/Cys)-based enzyme inhibitors. (Ser/Cys)-based enzyme inhibitors can interfere with lipid metabolism by impairing the activity of lipolytic enzymes.[12,28,37,40,48,55-57] To confirm whether mycobacterial (Ser/Cys)-based enzymes are involved in ILI mobilization after a 24 h-culture of *M. abscessus* S in MSM-NL (to induce ILI accumulation), lipid-rich mycobacteria were harvested, resuspended in fresh MSM-NL, and treated with either **HPOX$_{\text{yne}}$** or **CyC$_{\text{31yne}}$**. Apolar lipids were extracted and the TAG content was analyzed by thin layer chromatography (TLC) (**Figure 1D**). Following 24 h incubation with **HPOX$_{\text{yne}}$** or **CyC$_{\text{31yne}}$**, a

significant reduction in TAG levels of 28.6% and 22.6% (p-value < 0.01), respectively, was reached compared to the untreated bacteria.

These findings indicate that the two click-ready ABPs impair TAG production, presumably through the inhibition of (Ser/Cys)-based enzymes. Consequently, they can be exploited as activity-based probes in a click-chemistry activity-based protein profiling (CC-ABPP) strategy, to identify the (Ser/Cys)-based enzymes involved in such lipid metabolism pathway.

OX and CyC click-ready probes allow identifying potential enzymes involved in TAG accumulation. To gain access to putative enzymes involved in ILI metabolism, lipid-rich (*i.e.*, MSM-NL) and lipid-poor (*i.e.*, MSM) *M. abscessus* S cultures were subjected to the chemoproteomic CC-ABPP approach using the two alkyne-containing inhibitors (**Figure 2A**). After either 24 h or 48 h of culture in MSM or MSM-NL, the bacteria were centrifuged and the pellets resuspended in fresh medium in presence of **HPOX$_{yne}$**, **CyC$_{31yne}$**, or DMSO (control) for an additional 24 h incubation at 37 °C. Following cell lysis, click-chemistry reaction between the obtained **HPOX$_{yne}$**- or **CyC$_{31yne}$**-enzyme complexes and the Desthiobiotin-N_3 *via* copper(I)-catalyzed Huisgen's 1,3-dipolar cycloaddition reaction afforded a stable triazole ring.[27] Enrichment on streptavidin agarose-beads followed by subsequent digestion with trypsin yielded peptides that were analyzed by liquid chromatography-tandem mass spectrometry (LC-MS/MS), and quantified by label-free quantitative analysis (**Figure 2A**).

A first comparative proteomic analysis between each control sample (*i.e.*, DMSO-treated *M. abscessus* for non-specific binding to streptavidin agarose-beads) at the two time-points and the APB-treated samples led to a first set of target enzymes with **HPOX$_{yne}$** and **CyC$_{31yne}$**, respectively, when applying p-value ≤0.01 and Fold change (Log_2) ≥1.0 thresholds on the proteomic analysis results (**Tables S1-S4**). Each of these first data sets, *i.e.*, the target proteins of **HPOX$_{yne}$** and **CyC$_{31yne}$** identified in MSM-NL culture of *M. abscessus* at 24 h and 48 h incubation, was further refined by means of a second comparative proteomic analysis using the data obtained from the same fishing experiments carried out in MSM (**Tables S1-S4**). The resulting mycobacterial targets of **HPOX$_{yne}$**

displayed as volcano plots (**Figure 2B**) and **CyC$_{31yne}$**, highlight the proteins captured by the two ABPs that were significantly more abundant in MSM-NL *vs*. MSM (*p*-value ≤0.05 and Fold change (Log_2) ≥1.0), and thus involved in physiological processes directly related to nitrogen-deprived condition and ILI-rich phenotype. As shown in the Venn diagram (**Figure 2C, upper panel**), using **HPOX$_{yne}$** as a probe, 26 and 236 enzymes were found to be differentially captured after 24 and 48 h of incubation in MSM-NL, respectively, with 14 proteins conserved over time. Most of the identified proteins belonged to the categories of conserved hypothetical proteins (4 / 26 and 35 / 236), cell wall/cell processes (2 / 26 and 14 / 236), intermediary metabolism/respiration (7 / 26 and 129 / 236), and global lipid metabolism (12 / 26 and 43 / 236). Among the 14 conserved identified enzymes, 10 belonged to the global lipid metabolism functional category and 4 to the intermediary metabolism/respiration (**Table S5** and **Figure 2C, upper panel**).

With **CyC$_{31yne}$** as a probe, the 12 and 64 captured proteins after 24 h and 48 h incubation in MSM-NL (**Figure 2C, lower panel**), respectively (**Table S6**), showed a comparable distribution profile. As observed above, these identified proteins mainly belonged to the functional categories of conserved hypothetical proteins (1 / 12 and 2 / 64), cell wall/cell processes (4 / 12 and 4 / 64), intermediary metabolism/respiration (1 / 12 and 21 / 64), and global lipid metabolism (5 / 12 and 36 / 64).

Seven proteins were conserved over time, 4 of which belonging to the cell wall/cell processes and 3 to the global lipid metabolism functional categories (**Table S6**). Such distribution profiles agree with previous competitive ABPP experiments conducted with **OX** and **CyC** on *M. tuberculosis* and *M. abscessus* cultures.[30-33] To further focus on enzymes potentially involved in ILI metabolism, and considering that orthologs usually perform equivalent functions in the respective organisms,[8] the corresponding orthologs in the *M. tuberculosis* H37Rv genome of all identified proteins were reported using the KEGG database. These data were cross-referenced with the Uniprot (https://www.uniprot.org/) and Mycobrowser (https://mycobrowser.epfl.ch/) databases, providing reliable predictions of gene function in terms of essentiality, genomic location and activity.

The results of this differential pathway analysis identified 52 and 46 enzymes, captured by **HPOX$_{yne}$** and **CyC$_{31yne}$**, respectively, that may potentially be involved in the global lipid metabolism associated with ILI accumulation (**Figure 2D** and **Tables S7-S10**). A mostly comparable distribution of the captured enzymes involved in lipid catabolism/anabolism was obtained at 24 h and 48 h in MSM-NL, as shown in the Venn diagrams for each inhibitor probe (**Figure 2D**). A posteriori, this is not really surprising since these two probes target (Ser/Cys)-based enzymes by forming a covalent bond with the catalytic serine or cysteine residue.[23] In addition to these 33 common targets, 19 and 13 additional specific target enzymes were obtained with **HPOX$_{yne}$** (**Tables S7-S8**) and **CyC$_{31yne}$** (**Tables S9-S10**), respectively (**Figure 2D**).

The full list of these target enzymes is shown in **Table 1**, confirming the complementary selectivity of these two families of inhibitors with respect to the enzymes they capture. Of these 65 enzymes, 4 were captured only at 24 h, 46 only at 48 h, and 15 were fully conserved at both time points (**Figure 2E**), implying a dynamic process of ILI biosynthesis[2-3] with mostly different protein partners recruited over time.[58]

The identified proteins covered nearly all functional categories listed under the pathways related to *M. abscessus* lipid metabolism, ranging from biosynthesis of unsaturated fatty acids (2 proteins), cell wall/cell processes (4 proteins), ether lipid metabolism (1 protein), fatty acid biosynthesis (6 proteins), fatty acid metabolism/degradation (23 proteins), glycerolipid metabolism (6 proteins), glycerophospholipid metabolism (1 protein), lipid biosynthesis proteins (6 proteins), and peptidoglycan biosynthesis (1 protein). Additional sets of 10 proteins involved in lipid metabolism and 4 proteins belonging to intermediary metabolism and respiration have also been included (**Table 1**).

In agreement with previous work, 41 / 65 (63%) proteins had already been identified *via* competitive ABPP with **OX** and **CyC** molecules either on culture and/or total lysate of *M. abscessus*[30-31] and *M. tuberculosis*,[32-33,47] thus confirming the robustness of this bio-orthogonal CC-ABPP direct approach. These included five Cutinase-like proteins (MAB_0178; MAB_3763; Mab_3765;

MAB_3766; MAB_3809c); two Lip-family members (MAB_2814; MAB_3447c); a possible α/β-fold hydrolase (MAB_3810); two putative methyltransferases (MAB_4328c; MAB_4587c); the probable D-alanyl-D-alanine carboxypeptidase DacB (MAB_3234); the β-ketoacyl-ACP synthase III (MAB_1141c); and several members of the antigen 85 complex (MAB_0175; MAB_0176; MAB_177) (**Table 1**).

Given our *in vitro* model of ILI accumulation based on nitrogen starvation in presence of glycerol as the sole carbon source, glycerolipid and glycerophospholipid metabolism thus plays a central role in TAG production.[2] Accordingly, key enzymes in the regulation of glycerol uptake and metabolism were identified. These include the glycerol kinase Glpk (MAB_0382) and the Glycerol-1-phosphatase (MAB_2357) which participate in the conversion of glycerol to glycerol-3-phosphate; and the glycerol-3-phosphate dehydrogenase GlpD2 (MAB_3655c) involved in the reduction of glycerol-3-phosphate to generate glycerone phosphate.

In addition to these proteins, 38 / 65 (58.5%) enzymes were found directly associated with fatty acid biosynthesis, metabolism and degradation. Among these, the essential type I fatty-acid synthase (MAB_1512), four putative acyl-CoA synthetase/ligase (MAB_0179; MAB_1978c; MAB_3592c; MAB_4055c), two probable acyl-CoA thiolase (MAB_0850; MAB_1192c), four probable acetyl-CoA acetyltransferase (MAB_0612c; MAB_1463; MAB_2042c; MAB_3455c), four probable enoyl-CoA hydratase/isomerase (MAB_0981c; MAB_1069c; MAB_1187c; MAB_3350), thirteen probable acyl-CoA dehydrogenase (MAB_0065c; MAB_0255; MAB_0328; MAB_0851; MAB_1188c; MAB_2085; MAB_3040c; MAB_3481; MAB_3636c; MAB_3860c; MAB_4336; MAB_4437; MAB_4609c), and two dehydrogenases (MAB_0598; MAB_0983c) were identified (**Table 1**). Four additional proteins annotated as the acetyl-coenzyme A synthetase (MAB_0425c), two polyketide synthases (MAB_1140; MAB_2212), and the putative cyclopropane-fatty-acyl-phospholipid synthase (MAB_0310c) were also identified. Finally, our differential proteomic analysis has highlighted the presence of the putative long-chain acyl-CoA synthase MAB_2348. This protein is indeed homologous to the bifunctional long-chain acyl-CoA synthase/lipase BCG_1721 (65%

sequence identity) which has been reported as an important regulator of TAG levels and so in ILI formation in *M. bovis* BCG.[4]

In 2019, Dubois *et al*. reported the *M. abscessus* transcriptome both in an amoebic environmental host and in infected murine macrophages.[59] Interestingly, the genes encoding the fatty acid-CoA synthase MAB_4055c, the acyl-CoA dehydrogenase MAB_4437, and the two acetyl-CoA transferases MAB_0612c and MAB_3455c were among the 15 genes up-regulated in both *M. abscessus*-infected amoebae and murine macrophages, suggesting their potential role in the biochemical activation and β-oxidation of fatty acids upon infection (**Table 1**). Interestingly, 6 of the captured proteins in this study (MAB_0255, MAB_0310c, MAB_1512, MAB_1978c (FadD15), MAB_2348, and MAB_4609c) were also among the 28 proteins belonging to the lipid metabolism functional category reported as core components of the *M. tuberculosis* ILI-associated proteome.[8]

Recently, using APEX2 proximity labeling technology applied to the MSM-NL *in vitro* model of ILI accumulation with *M. abscessus* S, we identified 228 proteins potentially involved in ILI biosynthesis, of which 45 candidate proteins were annotated as part of the lipid metabolism pathway.[58] Of interest, 18 out of these 45 proteins were also identified with the **OX$_{yne}$** and **CyC$_{yne}$** ABPs (**Table 1**). These included the essential type I fatty-acid synthase (MAB_1512), two acyl-CoA ligases (MAB_0179; MAB_1978c), the two acyl-CoA thiolases (MAB_0850; MAB_1192c), the acetyl-CoA acetyltransferase (MAB_1463), six acyl-CoA dehydrogenases (MAB_0065c; MAB_0255; MAB_0851; MAB_3040c; MAB_3481; MAB_4437), the acyl-CoA hydratase (MAB_1187c), the polyketide synthase Pks5 (MAB_2212), the antigen 85C (MAB_0175), the 3-oxoacyl-[acyl-carrier-protein] reductase (MAB_0952), and two proteins involved in glycerol metabolism (MAB_3400; MAB_3655c) (**Table 1**). Among them, the enoyl-CoA hydratase MAB_1187c and the three acyl-CoA dehydrogenases MAB_3040c, MAB_3481 and MAB_4437, were shown to successfully colocalize with Nile Red-stained ILI.[58] In addition, deletion of the corresponding genes for *MAB_1187c*, *MAB_3040c*, and *MAB_3481*, resulted in a modest (28-33%) reduction in TAG levels, suggesting an indirect or secondary role in TAG accumulation. This also

suggests that other proteins may be involved in these processes, providing redundant functionality. However, the *MAB_4437* gene, which is up-regulated upon *M. abscessus* infection,[59] had no effect on lipid accumulation, as its deletion did not alter TAG levels compared to the wild-type strain.[58] The fact that these later four enzymes are also captured by our inhibitor probes reinforces the relevance of the CC-ABPP approach to identify major actors in TAG biosynthesis and ILI catabolism/anabolism.

Overall, the diversity of proteins identified under these nitrogen-limiting conditions suggests that TAG accumulation in the form of ILI may not be limited to energy storage, but might also provide a source of lipids dedicated to maintaining the overall cellular homeostasis of mycobacteria under stringent conditions.[2] Most importantly, these results underscore the complementarity of the **OX** and **CyC** in targeting (Ser/Cys)-based enzymes and therefore their added-value as activity-based probes to identify key mycobacterial enzymes involved in ILI accumulation by ABPP approaches. This will enlighten our understanding of the metabolic pathways used by pathogenic mycobacteria to catabolize host-derived lipids for survival.

The long chain-fatty-acid--CoA ligase MAB_1978c (FadD15) is involved in TAG production and ILI accumulation. Given the moderate results obtained with the deletion mutant strains of MAB_1187c, MAB_3040c, MAB_3481 and MAB_4437,[58] and to further investigate the impact of the identified enzymes on TAG accumulation, we focused on *i*) non-essential genes with orthologs in *M. tuberculosis* (≥50% sequence identity), and *ii*) candidate genes that do not encode putative proteins that might have redundant function. Taking these criteria into account, MAB_1978c (FadD15), also identified with the APEX2 proximity labeling approach,[58] was selected to investigate its involvement in ILI accumulation.

FadD15 is a non-essential putative long-chain-fatty-acid--CoA ligase that is functionally categorized as being involved in lipid metabolism. Like its *M. tuberculosis* ortholog Rv2187,[60] FadD15 is assumed to play a central role in global lipid metabolism. Indeed, FadD15 is predicted to act at the

termination of the fatty acid biosynthesis pathway [KEGG PATH:mab00061] with no alternative proteins that could perform its activity. It appears to be the only enzyme that catalyzes the activation of long-chain fatty acids as acyl-CoA, which would be further processed for elongation, glycerolipid and/or glycerophospholipid biosynthesis, or recycled *via* the β-oxidation pathway [KEGG PATH:mab00071]. In addition, the fact that Rv2187 is part of the core component of the *M. tuberculosis* ILI-associated proteome,[8] strengthens its involvement in ILI biosynthesis and supports its selection for validation experiments.

A deletion mutant, designated Δ*fadD15,* was generated by using a two-step homologous recombination procedure using the pUX1-*katG* vector (**Figure S3**).[61] Its complemented counterpart Δ*fadD15*::C was obtained using the pVV16::*fadD15-sfGFP* complementation plasmid that allows the constitutive production of recombinant MAB_1978c fused to a superfolder Green Fluorescent Protein (*sf*GFP)-tag under the control of the *hsp60* promoter. In parallel, *fadD15* was also cloned and overexpressed in *M. abscessus* S strain using the same pVV16::*fadD15-sfGFP* for subsequent fluorescence microscopy experiments (**Figure S4**). First, when grown in 7H9TG^{OADC}, MSM or MSM-NL for 72 h at 37 °C, no significant differences in growth rate were observed between the *M. abscessus* wild-type and Δ*fadD15* (**Figure S5**), in agreement with the non-essentiality annotation of the *fadD15* gene in *M. abscessus* genome.[62]

Then, each strain was grown in MSM-NL for 24 h and 48 h, and then processed for apolar lipids TLC analysis (**Figure 3A**). At the two time points, quantitative densitometry revealed that TAG production was impaired by 46.7 ± 1.4% and 56.1 ± 2.5% (p-value < 0.0001) in Δ*fadD15* after 24 and 48 h of incubation in MSM-NL, respectively, as compared to the WT strain (**Figures 3A** & **S4C**). In contrast, complete restoration of TAG levels, *i.e.*, 102.9 ± 2.6% and 95.2 ± 2.7%, at 24 and 48 h, respectively, was achieved upon complementation in Δ*fadD15*::C. Moreover, the *M. abscessus* S_*fadD15-sfGFP* overexpressing strain induced a slight but significant increase in TAG levels by 1.08-fold (p-value < 0.05) as compared to the WT strain. Interestingly, the Δ*fadD15* showed comparable TAG levels to a triacylglycerol synthase 1 deletion mutant (Δ*tgs1*) in *M. abscessus* cultured in the MSM-

NL, as reported in a previous study.[12] Indeed, it has been clearly demonstrated that TAG accumulation in the form of ILI was *tgs1*-dependent, in *M. tuberculosis*,[63-64] *M. marinum*,[14] and in *M. abscessus*.[12-13] Moreover, this major TAG synthase has also been identified on the surface of mature ILI in *M. bovis* BCG,[4] underscoring its major contribution in ILI formation.

To confirm that these variations in TAG levels correlate with ILI accumulation, the 48 h cultures in MSM-NL were harvested, fixed with 4% paraformaldehyde, then stained with Nile Red and processed for fluorescence microscopy (**Figure 3B**). Nile Red-positive intrabacterial lipid structures were easily detectable in both the WT and Δ*fadD15*::C strains whereas such structures were mostly absent in the Δ*fadD15* mutant. Indeed, this mutant mainly displayed a weaker, peripheral staining pattern similar to the one observed for the WT strain grown in MSM medium. Quantitative analysis of the Nile Red fluorescence signal at the single bacterium level (**Figure 3B**) revealed that after 48 h of culture in MSM-NL medium, ILI accumulation was reduced by 47% in Δ*fadD15* (average mean pixel intensity [a.u.] of 53. 5 ± 1.2) as compared to WT (mean pixel intensity [a.u.] of 100.7 ± 3.0), whereas Δ*fadD15*::C (mean pixel intensity [a.u.] of 82.6 ± 1.7) restored the ILI-positive phenotype.

To assess the subcellular localization of the FadD15 protein during ILI formation, *M. abscessus* S_*fadD15-sfGFP* overexpressing strain was grown in MSM-NL or MSM for 48 h and processed for fluorescence microscopy, as described above. As observed previously with the fluorescent inhibitor probes, in MSM a diffuse and mainly peripheral fluorescence signal was observed, suggesting a homogeneous distribution of the labelled FadD15-*sf*GFP protein in the lipid-poor bacteria (**Figure S7**). Conversely, *M. abscessus* S_*fadD15-sfGFP* cultured in MSM-NL displayed clear, intense and compact Nile Red ILI-positive areas, which colocalized with the *sf*GFP fluorescent signal (**Figure 3C**). Statistical analysis confirmed the overlap between green (*sf*GFP) and red pixel (Nile Red) with Pearson's correlation coefficients and Manders' colocalization coefficients[53] of 0.924 and 0.982, respectively; a Costes *p*-value[54] of 1 and Li's ICQ value[52] of 0.435.

All these results demonstrated the clear involvement of MAB_1978c/FadD15 in TAG production and subsequent ILI formation *in vitro*. More globally, the fact that glycerol is the sole carbon source

available in our MSM-NL model implies the use of well conserved pathways to synthesize TAG.[65] Consequently, from the set of the 65 captured proteins with both **HPOX$_{yne}$** and **CyC$_{31yne}$**, and literature data on *M. tuberculosis*[66-67] and *M. abscessus*[59] transcriptomic studies, it is possible to map some enzymes involved in *M. abscessus* lipid metabolism related to TAG formation and accumulation through ILI (**Figure 4**).

The initial step would consist in the *de novo* biosynthesis of fatty acyl-compounds in the form of acyl-CoAs through the action of the type I fatty acid synthase (FAS-I) as well as all enzymes necessary for the biochemical activation and β-oxidation of fatty acids: fatty acid-CoA synthase/ligase (FadD3,13,15,32), acyl-CoA dehydrogenase (FadE2,5,6,7,8,9,20), enoyl-CoA hydratase (EchA7), hydroxybutyryl-CoA dehydrogenase (FadB), and acetyl-CoA transferase (FadA3,4,5,6). However, given the energetic costs associated with such *de novo* fatty acid biosynthesis in MSM-NL, where glycerol is the sole carbon source, it is likely that other rearrangements of lipid metabolism, such as phospholipid recycling through the action of some Cutinase-like proteins (*e.g.*, Cut4),[68-69] may led to fatty acid precursors that could be incorporated into biosynthetic pathways *via* the β-oxidation pathway. The second step is the formation of glycerol-3-phosphate (G3P) substrates generated by the action of the glycerol kinase (GlpK). Finally, the sequential acylation of the G3P substrates with the latter fatty acyl-CoA residues is mediated by the enzymes from the Kennedy pathway. These may include the bifunctional long-chain acyl-CoA synthase/lipase (MAB_2348), whose *M. bovis* BCG ortholog[4] has been demonstrated to be involved in long-chain TAG and ILI formation processes when assessed under non-replicating conditions. In addition, the Ag85A/B/C complex proteins, which express diacylglycerol acyltransferase (DGAT) activity and mediate the transesterification of diacylglycerol with long-chain acyl-CoA, are also important contributors to TAG synthesis.[45]

CONCLUSION

Using an *in vitro* model based on nitrogen deprivation to promote TAG accumulation and subsequent production of lipid-loaded *M. abscessus* cells, together with two selective multitarget inhibitors

belonging to the **OX** and **CyC** distinct families, we identified a set of 65 enzymes that may directly or indirectly participate in these processes. We have validated this approach by demonstrating that the long-chain-fatty-acid--CoA ligase MAB_1978c/FadD15 colocalizes with ILI and acts as a major actor in ILI formation. In addition, the fact that the enoyl-CoA hydratase MAB_1187c as well as the three acyl-CoA dehydrogenases MAB_3040c (FadE20), MAB_3481 (FadE4) and MAB_4437 (FadE5), have been identified by two distinct experimental approaches and further validated as essential actors in TAG accumulation,[58] confirms the functionality of our ABPP-based method to probe mycobacterial lipid metabolism. More work remains to be done to fully characterize and validate the other proteins identified *via* ABPP to provide a clear picture of their specific role(s) in ILI metabolism.

Overall, our data confirm the importance of fatty acid and lipid metabolism in *M. abscessus* under nutritional stress and highlight the importance of proteins involved in TAG mobilization as potential therapeutic targets. Nevertheless, one needs to consider that the nutrients available *in vivo* differ from the *in vitro* conditions described here, as mycobacteria can be found in different cellular compartments (*e.g.* phagosome, macrophage, granulomas, etc.) during infection. In particular, mycobacteria can reside in highly lipidic environments, such as those encountered in foamy macrophages, providing access to host lipids to build up TAGs which are subsequently stored into ILI.[3]

In summary, the multi-targeted **OX** & **CyC** inhibitors represent powerful probes for monitoring mycobacterial infection and identifying key specific targets within infected macrophages. Their use as specific activity-based probes to identify the mycobacterial lipolytic enzymes involved in host lipid bodies degradation, lipid accumulation in ILI, as well as in the consumption of these intrabacterial lipids using the model of infected foamy and non-foamy macrophages,[6,11,25] opens new opportunities. The knowledge acquired by working on living infected cells should provide crucial information on the life cycle of intracellular mycobacteria, and inspire new therapeutic strategies to counter latent/persistent bacilli in infected individuals.

Finally, our approach can be applied to multiple organisms, biological contexts and situations, and, therefore, is of interest for a wide range of scientists relying on advanced chemical-biology to understand bacterial pathogenesis.

METHODS

Chemistry

Synthesis of OX and CyC activity-based probes. The Cyclipostins analogs **CyC$_{31}$**, **CyC$_{31yne}$** and **CyC$_{31\text{-}Dansyl}$**, as well as the Oxadiazolone derivative **HPOX**, were synthesized as described previously.[32,35,47] Detailed procedures and the full chemical characterization (^{1}H and ^{13}C NMR spectra) of the new **OX** probes (*i.e.*, **HPOX$_{yne}$** and **HP$_{\text{-}NBD\text{-}}$OX**) are reported in **Supporting Information**. Stock solutions (10 mM) in which the **OX** & **CyC** molecules (purity of ≥95%) were found to be completely soluble in dimethyl sulfoxide (DMSO) were prepared and stored at 4 °C.

Biological evaluation

All detailed Material and Methods are given in **Supporting Information**.

Bacterial strains and growth conditions. *M. abscessus* CIP104536^{T} with either a smooth (S) or a rough (R) morphotype, was classically grown in Middlebrook 7H9 liquid medium (BD Difco, Le Pont de Claix, France) supplemented with 0.05% Tween 80 (Sigma-Aldrich, Saint-Quentin Fallavier, France), 0.2% glycerol (Euromedex, Souffelweyersheim, France) and 10% oleic albumin dextrose catalase (OADC enrichment, BD Difco, Le Pont de Claix, France) (7H9-S^{OADC}) at 37 °C and 200 rpm.

Generation of lipid-loaded cells. ILI accumulation in *M. abscessus* S liquid culture was performed as previously reported[12] following 24 or 48 h incubation period at 37 °C and 200 rpm using either Mineral Salt Medium (MSM) (2 g/L Na_2HPO_4, 1 g/L KH_2PO_4, 0.5 g/L NaCl, 0.2 g/L $MgSO_4$, 20 mg/L $CaCl_2$, 1 g/L NH_4Cl, and 5% glycerol) or Mineral Salt Medium Nitrogen Limiting (MSM-

NL) containing only 0.15 g/L NH_4Cl. Alternatively, after 24 h incubation period, the latter cultures were centrifuged and the pellets resuspended in respective fresh MSM or MSM-NL at a final theoretical OD_{600} of 20. One mL sample of these homogeneous bacterial suspensions was incubated with **CyC$_{31yne}$** (200 µM final concentration), **HPOX$_{yne}$** (500 µM final concentration) or DMSO (control), as well as with the fluorescent **CyC$_{31\text{-}Dansyl}$** or **HP$_{\text{-}NBD\text{-}}$OX** probes (100 µM final concentration) for additional 24 h.

Normalization, lipid extraction and thin layer chromatography (TLC) analysis. At 24 and 48 h incubation period, *M. abscessus* S cultures in MSM or MSM-NL, in presence or absence of inhibitor, were centrifuged. Pellets were lyophilized overnight and weighed to obtain the exact dry weight of the mycobacterial residue. Apolar lipids were extracted as previously reported,[12] and further analyzed using glass TLC plates (TLC Silica Gel 60 F_{254}, Merck) and petroleum ether (40-60 °C fraction)/diethyl ether (90:10, *v*/*v*) as eluent. Following revelation with a cupric acetate-orthophosphoric acid solution, each resolved plate was scanned using a Chemidoc™ MP Imaging System (Bio-Rad, Marnes-la-Coquette, France), and densitometric analyses were performed using the ImageLab software version 5.2 (Bio-Rad) to determine relative TAG content per sample (see **Figure S8** for an example of quantification of TAG level).

MIC determination. The antibacterial activity of the fluorescent **CyC$_{31\text{-}Dansyl}$** and **HP$_{\text{-}NBD\text{-}}$OX**, as well as the **CyC$_{31yne}$** and **HPOX$_{yne}$** probes as compared to the parent **CyC$_{31}$** and **HPOX** against *M. abscessus* S & R growth, was assessed by determining their MICs in 96-well flat-bottom Nunclon Delta Surface microplates with lid (Thermo Fisher Scientific, Illkirch, France) using the REMA assay.[30-31,35,51] MIC values were determined by fitting the relative fluorescence unit (RFU%) sigmoidal dose-response curves in Kaleidagraph 4.2 software (Synergy Software, Reading, PA, USA). The lowest compound concentration leading to 50% and 90% growth inhibition was defined

as the MIC_{50} and MIC_{90}, respectively. Amikacin (AMK) and Imipenem (IMP) were used as reference drugs.

Activity-based protein profiling (ABPP) experiments – adapted from [47].

Capture of M. abscessus S potential target enzymes from $HPOX_{yne}$ and CyC_{31yne}-treated MSM and MSM-NL culture. After 24 h or 48 h incubation period in MSM or MSM-NL at 37 °C and 200 rpm, the culture was centrifuged and the pellets were resuspended in fresh MSM or MSM-NL at a final theoretical OD_{600} of 20. One mL sample of these homogeneous bacterial suspensions was incubated with **CyC_{31yne}** (200 µM final concentration), **$HPOX_{yne}$** (500 µM final concentration) or DMSO (control) at 37 °C for additional 24 h under shaking at 200 rpm. Bacteria were washed, resuspended in PBS buffer at a 1:1 (*w/v*) ratio and lysed by mechanical disruption using Mini-Beadbeater-96 (BioSpec, Bartlesville, OK, USA). Both **CyC_{31yne}-** and **$HPOX_{yne}$-**treated *M. abscessus* and DMSO-control lysate samples (500 µL – 0.5 mg total proteins) were subjected to click-chemistry reaction by successive addition of Desthiobiotin-PEG_3-N_3 (#CLK-AZ104P4-100, Jena Bioscience, Jena, Deutschland; 40 mM in DMSO), TBTA ligand (1.667 mM *t*BuOH/DMSO 80:20, *v/v*) and fresh TCEP (50 mM H_2O) solution (Sigma-Aldrich), and fresh $CuSO_4$ solution (50 mM in H_2O). Samples were further processed for affinity enrichment with Pierce™ High-Capacity Streptavidin Agarose Resin (Thermo Fisher Scientific ref. 20359), according to the manufacturer's instructions. The resulting captured biotinylated proteins solution was mixed with 5X Laemmli reducing sample buffer, and heated at 95°C for 5 min.

Mass spectrometry analysis. The protein isolates were loaded and stacked on a NuPAGE gel (Thermo Fisher Scientific Invitrogen). Stained bands were digested with high sequencing grade trypsin (Promega, Madison, WI, USA).[31,47] Extracted peptides were reconstituted with 0.1% trifluoroacetic acid in 2% acetonitrile and analyzed by liquid chromatography (LC)-tandem MS (MS/MS) using a Q Exactive Plus Hybrid Quadrupole-Orbitrap online with a nanoLC Ultimate 3000 chromatography system (Thermo Fisher Scientific). Protein identification and quantification were processed using the

MaxQuant computational proteomics platform, version 1.6.3.4. using the *M. abscessus* (UP000007137) database extracted from UniProt (date 2023-03-10; 4,940 entries). The statistical analysis was done with Perseus program (version 1.6.15). Differential proteins were detected using a two-sample *t*-test using permutation-based FDR-controlled at 5 (**CyC$_{32yne}$**) and 1 (**HPOX$_{yne}$**) employing 250 permutations.

The mass spectrometry proteomics data have been deposited to the ProteomeXchange Consortium (www.proteomexchange.org) *via* the PRIDE partner repository (https://www.ebi.ac.uk/pride/login) with the dataset identifier PXD048770.

Fluorescence imaging of lipid-loaded *M. abscessus* cells

Nile Red staining. After 24 h and 48 h incubation period either in MSM or MSM-NL, and in presence/absence of inhibitors, *M. abscessus* S cultures were harvested, washed with PBS, then fixed with 4% paraformaldehyde and incubated with Nile Red fluorescent dye (Interchim, Montluçon, France) for ILI staining as previously described.[12]

Fluorescent Microscopy. Fixed stained samples (5 µL bacterial suspension, *i.e.*, 7.5×10^6 cells) processed for fluorescence imaging as described previously.[35]

Colocalization analysis between the Dansyl, NBD or GFP and Nile Red fluorescence using coloc2 plugin of ImageJ/Fiji. Colocalization between the Nile Red and Dansyl, NBD or GFP fluorescence intensity was assessed by evaluating the pixel intensity correlation over space using the Coloc2 plugin of ImageJ/Fiji.

Plasmid construction and cloning. All specific primers and plasmids used in this study are listed in **Supporting Information Tables S11-S12**. All cloned fragments were amplified using purified *M. abscessus* genomic DNA.

Construction of MAB_1978c mutant strains. Deletion mutant Δ*mab_1978c* (= Δ*fadD15*) was obtained using the double homologous recombination unmarked strategy developed by Richard *et*

al.[61] For complementation strain, the *fadD15* gene was amplified using the primer pairs *pVV16::fadD15-Fw* and *pVV16::fadD15-Rv*, then fused with superfolder Green Fluorescent Protein (*sfGfp*) gene, and cloned into pVV16 plasmid[44] to generate *pVV16::fadD15-sfGFP*. Sequence integrity of each construct was confirmed by DNA sequencing (Eurofins Genomics). All the constructs were further transformed in electrocompetent *M. abscessus* S_Δ*fadD15* strains. Alternatively, overexpressing mutant strain was built using the same *pVV16::fadD15-sfGFP* vector following transformation in electrocompetent *M. abscessus* S wild-type strain. Validation of Δ*fadD15* mutant was made by PCR amplification and DNA sequencing of the genomic region surrounding the site of gene deletion (**Table S11** & **Figure S3**).[61,70] The *M. abscessus* S_Δ*fadD15*::C complementation strain as well as the *M. abscessus* S*_fadD15-sfGFP* overexpressing strain were checked by PCR amplification and fluorescence microscopy (**Table S11** & **Figure S4**).

Functional validation of mab_1978c in TAG accumulation. The *M. abscessus* S_Δ*fadD15* deletion strain, the complemented *M. abscessus* S_Δ*fadD15*::C, and the overexpressing *M. abscessus* S*_fadD15-sfGFP* strains were cultured in MSM and MSM-NL, for their ability to accumulate TAG in the form of ILI. After 48 h incubation, all bacterial cultures were processed for TAG content analysis by TLC and fluorescence microscopy.

Statistical analysis. GraphPad Prism 8 (GraphPad Software, Boston, MA, USA) was used for all statistical analyses, as detailed in each figure legends. Differences were considered significant with calculated p-values ≤ 0.05.

ASSOCIATED CONTENT

* Supporting Information

Supporting Information for this article is available online

Tables S1-S12. Target proteins identified after a 24 h or 48 h culture of *M. abscessus* S in MSM-NL, through CC-ABPP by LC-ESI-MS/MS analysis, using **HPOX$_{yne}$** or **CyC$_{31yne}$** probes; and list of primers and plasmids used in this study (XLSX).

S1 Appendix. Detailed protocols regarding chemistry and biological evaluation. **Figure S1**, the **HP$_{-NBD-}$OX** and the **CyC$_{31-Dansyl}$** colocalized with ILI on *M. abscessus* S cultured in MSM-NL; **Figure S2**, controls for fluorescent microscopy imaging related to the colocalization of the fluorescent probes with ILI on culture of *M. abscessus* S in MSM-NL medium; **Figure S3**, unmarked deletion strategy for the deletion of *MAB_1978c* (*fadD15*) in *M. abscessus*; **Figure S4**, generation of the Δ*fadD15*::C complementation strain and *M. abscessus* S*_fadD15-sfGFP* overexpressing strain. **Figure S5**, growth curves of *M. abscessus* S wild-type and Δ*fadD15* deletion mutant in 7H9TG^{OADC}, MSM and MSM-NL, respectively; **Figure S6**, controls for fluorescent microscopy imaging related to the colocalization of FadD15-*sf*GFP with ILI on culture of *M. abscessus* S*_fadD15-sfGFP* overexpressing strain in MSM-NL medium; **Figure S7**, *M. abscessus* S*_fadD15-sfGFP* overexpressing strain displays a diffuse fluorescence when grown in MSM medium; **Figure S8**, typical example of quantification of TAG level from a TLC using the ImageLab software *v*.5.2; **Figure S9**, NMR spectra of the new **HPOX$_{yne}$** and **HP$_{-NBD-}$OX** compounds. (PDF).

AUTHOR INFORMATION

Corresponding Author

Jean-François Cavalier - Aix-Marseille Univ, CNRS, LISM, IMM FR3479, Marseille, France. https://orcid.org/0000-0003-0864-8314; Email: jfcavalier@imm.cnrs.fr.

Authors

Romain Avellan - Aix-Marseille Univ, CNRS, LISM, IMM FR3479, Marseille, France.

Jordan Lehoux - IBMM, Univ Montpellier, CNRS, ENSCM, Montpellier, France.

Thomas Francis - Aix-Marseille Univ, CNRS, LISM, IMM FR3479, Marseille, France.

Tonia Dargham - Aix-Marseille Univ, CNRS, LISM, IMM FR3479, Marseille, France; and IHU Méditerranée Infection, Aix-Marseille Univ., Marseille, France

Léa Celik - Aix-Marseille Univ, CNRS, LISM, IMM FR3479, Marseille, France.

Alexandre Guy - IBMM, Univ Montpellier, CNRS, ENSCM, Montpellier, France

Isabelle Poncin - Aix-Marseille Univ, CNRS, LISM, IMM FR3479, Marseille, France

Vanessa Point - Aix-Marseille Univ, CNRS, LISM, IMM FR3479, Marseille, France

Laurent Kremer - Centre National de la Recherche Scientifique UMR 9004, Institut de Recherche en Infectiologie de Montpellier (IRIM), Université de Montpellier, 1919 route de Mende, 34293, Montpellier, France; and INSERM, IRIM, 34293 Montpellier, France. https://orcid.org/0000-0002-6604-4458

Thierry Durand - IBMM, Univ Montpellier, CNRS, ENSCM, Montpellier, France. https://orcid.org/0000-0001-6086-7296

Stéphane Audebert - INSERM, CNRS, Institut Paoli-Calmettes, CRCM, Marseille Protéomique, Aix-Marseille University, France. https://orcid.org/0000-0002-9409-2588

Luc Camoin - INSERM, CNRS, Institut Paoli-Calmettes, CRCM, Marseille Protéomique, Aix-Marseille University, France. https://orcid.org/0000-0002-1230-4787

Christopher D. Spilling - Department of Chemistry and Biochemistry, University of Missouri-St. Louis, MO, USA

Pierre Santucci - Aix-Marseille Univ., CNRS, LISM UMR7255, IMM FR3479, Marseille, France. https://orcid.org/0000-0002-6291-3425

Céline Crauste - IBMM, Univ Montpellier, CNRS, ENSCM, Montpellier, France. https://orcid.org/0000-0002-5714-8749

Stéphane Canaan - Aix-Marseille Univ., CNRS, LISM UMR7255, IMM FR3479, Marseille, France. https://orcid.org/0000-0001-7478-300X

Author Contributions

Conceptualization: S.C. and J.-F.C. Data curation: S.A. and L.Ca. Resources: J.L., A.G., T.Du., C.C. and C.D.S. Investigations: R.A., T.F., T.Da., L.Ce., S.A., L.Ca., I.P. and V.P. Formal analysis: R.A., T.F., T.Da., S.A., L.Ca., P.S., S.C. and J.-F.C. Visualization: R.A., T.F., T.Da. and J.-F.C. Writing-original draft: J.-F.C. Writing-review & editing: R.A., J.L., T.F., T.Da., L.Ce., A.G., I.P., V.P., L.K., T.Du., S.A., L.Ca., C.D.S., P.S., C.C., S.C. and J.-F.C. Supervision: S.C. and J.-F.C. Funding acquisition: S.C. and J.-F.C. Validation: J.-F.C. Project administration: J.-F.C.

R.A., J.L. T.F. and T.Da. contributed equally and should be considered as first coauthors. All authors have given approval to the final version of the manuscript.

Declaration of interests

The authors declare no competing interests.

ACKNOWLEDGEMENTS

This work was supported by the CNRS, Aix Marseille University, and the Agence Nationale de la Recherche (LipInTB project N°ANR-19-CE44-0011, and ILIome project N°ANR-20-CE44-0019). Proteomics analyses were done using the mass spectrometry facility of Marseille Proteomics (marseille-proteomique.univ-amu.fr) supported by IBISA, the Cancéropôle PACA, the Provence-Alpes-Côte d'Azur Region, the Institut Paoli-Calmettes, and Fonds Européen de Développement Regional (FEDER). R.A. PhD fellowship was supported by the Agence Nationale de la Recherche (LipInTB project N°ANR-19-CE44-0011). T.D. PhD fellowship was funded by the foundation IHU Méditerranée Infection. J.L. and T.F. PhD fellowships are supported by the Ministère de l'Enseignement Supérieur et de la Recherche Française. The authors wish also to thank Dr Wassim Daher (IRIM, Montpellier, France) for his valuable input and discussions. J-F.C. is particularly grateful to Deezer and Carte Noire coffee for their invaluable help and support during the writing of this manuscript.

ABBREVIATIONS

ABP, activity-based probe; ABPP, activity-based protein profiling; au, arbitrary unit; AMK, amikacin; CC-ABPP, click-chemistry activity-based protein profiling; CC_{50}, compound concentration leading to 50% of cell cytotoxicity; CyC, Cyclipostins and Cyclophostin analogues; ILI, intrabacterial lipid inclusion; IMP, imipenem; MIC_{50}/MIC_{90}, minimal inhibitory concentration leading to 50% or 90% of growth inhibition; MSM, mineral salt medium; MSM-NL, mineral salt medium nitrogen limiting; NTM, nontuberculous mycobacterial; REMA, resazurin microtiter assay; OX, oxadiazolone derivatives; TAG, triacylglycerol; TB, tuberculosis; TLC, thin layer chromatography; VLDL, very low-density lipoproteins.

REFERENCES

(1) Brennan, P. J., Structure, function, and biogenesis of the cell wall of *Mycobacterium tuberculosis*. *Tuberculosis* **2003**, *83* (1), 91-97.

(2) Mallick, I.; Santucci, P.; Poncin, I.; Point, V.; Kremer, L.; Cavalier, J.-F.; Canaan, S., Intrabacterial lipid inclusions in mycobacteria: unexpected key players in survival and pathogenesis? *FEMS Microbiol Rev* **2021**, *45* (6), fuab029.

(3) Dargham, T.; Mallick, I.; Raze, D.; Kremer, L.; Canaan, S., Chapter 12 - Intrabacterial lipid inclusions: overview of an amazing organelle. In *Biology of Mycobacterial Lipids*, Fatima, Z.; Canaan, S., Eds. Academic Press: 2022; pp 253-269. DOI: https://doi.org/10.1016/B978-0-323-91948-7.00003-8.

(4) Low, K. L.; Shui, G.; Natter, K.; Yeo, W. K.; Kohlwein, S. D.; Dick, T.; Rao, S. P.; Wenk, M. R., Lipid droplet-associated proteins are involved in the biosynthesis and hydrolysis of triacylglycerol in *Mycobacterium bovis* bacillus Calmette-Guerin. *J Biol Chem* **2010**, *285* (28), 21662-70.

(5) Daniel, J.; Maamar, H.; Deb, C.; Sirakova, T. D.; Kolattukudy, P. E., *Mycobacterium tuberculosis* Uses Host Triacylglycerol to Accumulate Lipid Droplets and Acquires a Dormancy-Like Phenotype in Lipid-Loaded Macrophages. *PLOS Pathogens* **2011**, *7* (6), e1002093.

(6) Caire-Brändli, I.; Papadopoulos, A.; Malaga, W.; Marais, D.; Canaan, S.; Thilo, L.; de Chastellier, C.; Flynn, J. L., Reversible Lipid Accumulation and Associated Division Arrest of *Mycobacterium avium* in Lipoprotein-Induced Foamy Macrophages May Resemble Key Events during Latency and Reactivation of Tuberculosis. *Infect Immun.* **2014**, *82* (2), 476-490.

(7) Hammond, R. J.; Baron, V. O.; Oravcova, K.; Lipworth, S.; Gillespie, S. H., Phenotypic resistance in mycobacteria: is it because I am old or fat that I resist you? *J Antimicrob Chemother* **2015**, *70* (10), 2823-7.

(8) Dargham, T.; Mallick, I.; Kremer, L.; Santucci, P.; Canaan, S., Intrabacterial lipid inclusion-associated proteins: a core machinery conserved from saprophyte Actinobacteria to the human pathogen Mycobacterium tuberculosis. *FEBS Open Bio* **2023**, *13* (12), 2306-2323.

(9) Mattos, K. A.; Oliveira, V. G.; D'Avila, H.; Rodrigues, L. S.; Pinheiro, R. O.; Sarno, E. N.; Pessolani, M. C.; Bozza, P. T., TLR6-driven lipid droplets in *Mycobacterium leprae*-infected Schwann cells: immunoinflammatory platforms associated with bacterial persistence. *J Immunol* **2011**, *187* (5), 2548-58.

(10) Bouzid, F.; Bregeon, F.; Poncin, I.; Weber, P.; Drancourt, M.; Canaan, S., *Mycobacterium canettii* Infection of Adipose Tissues. *Front Cell Infect Microbiol* **2017**, *7*, 189.

(11) Santucci, P.; Diomande, S.; Poncin, I.; Alibaud, L.; Viljoen, A.; Kremer, L.; de Chastellier, C.; Canaan, S., Delineating the Physiological Roles of the PE and Catalytic Domains of LipY in Lipid Consumption in Mycobacterium-Infected Foamy Macrophages. *Infect Immun* **2018**, *86* (9), 10.1128/iai.00394-18.

(12) Santucci, P.; Johansen, M. D.; Point, V.; Poncin, I.; Viljoen, A.; Cavalier, J. F.; Kremer, L.; Canaan, S., Nitrogen deprivation induces triacylglycerol accumulation, drug tolerance and hypervirulence in mycobacteria. *Sci Rep* **2019**, *9* (1), 8667.

(13) Viljoen, A.; Blaise, M.; de Chastellier, C.; Kremer, L., MAB_3551c encodes the primary triacylglycerol synthase involved in lipid accumulation in *Mycobacterium abscessus*. *Mol Microbiol* **2016**, *102* (4), 611-627.

(14) Barisch, C.; Soldati, T., Breaking fat! How mycobacteria and other intracellular pathogens manipulate host lipid droplets. *Biochimie* **2017**, *141*, 54-61.

(15) Robbe-Saule, M.; Foulon, M.; Poncin, I.; Esnault, L.; Varet, H.; Legendre, R.; Besnard, A.; Grzegorzewicz, A. E.; Jackson, M.; Canaan, S.; Marsollier, L.; Marion, E., Transcriptional adaptation of *Mycobacterium ulcerans* in an original mouse model: New insights into the regulation of mycolactone. *Virulence* **2021**, *12* (1), 1438-1451.

(16) Armstrong, R. M.; Carter, D. C.; Atkinson, S. N.; Terhune, S. S.; Zahrt, T. C., Association of Mycobacterium Proteins with Lipid Droplets. *J Bacteriol* **2018**, *200* (16), 10.1128/jb.00240-18.

(17) Lopeman, R. C.; Harrison, J.; Desai, M.; Cox, J. A. G., Mycobacterium abscessus: Environmental Bacterium Turned Clinical Nightmare. *Microorganisms* **2019**, *7* (3), 90.

(18) Nessar, R.; Cambau, E.; Reyrat, J. M.; Murray, A.; Gicquel, B., Mycobacterium abscessus: a new antibiotic nightmare. *J Antimicrob Chemother* **2012**, *67* (4), 810-8.

(19) Johansen, M. D.; Herrmann, J. L.; Kremer, L., Non-tuberculous mycobacteria and the rise of Mycobacterium abscessus. *Nat Rev Microbiol* **2020**, *18* (7), 392-407.

(20) Roux, A. L.; Viljoen, A.; Bah, A.; Simeone, R.; Bernut, A.; Laencina, L.; Deramaudt, T.; Rottman, M.; Gaillard, J. L.; Majlessi, L.; Brosch, R.; Girard-Misguich, F.; Vergne, I.; de Chastellier, C.; Kremer, L.; Herrmann, J. L., The distinct fate of smooth and rough *Mycobacterium abscessus* variants inside macrophages. *Open biology* **2016**, *6* (11), 160185.

(21) Catherinot, E.; Clarissou, J.; Etienne, G.; Ripoll, F.; Emile, J. F.; Daffe, M.; Perronne, C.; Soudais, C.; Gaillard, J. L.; Rottman, M., Hypervirulence of a rough variant of the Mycobacterium abscessus type strain. *Infect Immun* **2007**, *75* (2), 1055-8.

(22) Jönsson, B. E.; Gilljam, M.; Lindblad, A.; Ridell, M.; Wold, A. E.; Welinder-Olsson, C., Molecular epidemiology of *Mycobacterium abscessus*, with focus on cystic fibrosis. *J Clin Microbiol* **2007**, *45* (5), 1497-1504.

(23) Cavalier, J. F.; Spilling, C. D.; Durand, T.; Camoin, L.; Canaan, S., Lipolytic enzymes inhibitors: A new way for antibacterial drugs discovery. *Eur J Med Chem* **2021**, *209*, 112908.

(24) Daniel, J.; Kapoor, N.; Sirakova, T.; Sinha, R.; Kolattukudy, P., The perilipin-like PPE15 protein in *Mycobacterium tuberculosis* is required for triacylglycerol accumulation under dormancy-inducing conditions. *Mol Microbiol* **2016**, *101* (5), 784-794.

(25) Santucci, P.; Bouzid, F.; Smichi, N.; Poncin, I.; Kremer, L.; De Chastellier, C.; Drancourt, M.; Canaan, S., Experimental Models of Foamy Macrophages and Approaches for Dissecting the Mechanisms of Lipid Accumulation and Consumption during Dormancy and Reactivation of Tuberculosis. *Front Cell Infect Microbiol* **2016**, *6*, 122.

(26) Shukla, E.; D. Bendre, A.; M. Gaikwad, S., Hydrolases: The Most Diverse Class of Enzymes. In *Hydrolases*, Haider, S.; Haider, A.; Catala, A., Eds. IntechOpen: Rijeka, 2022. DOI: https://doi.org/10.5772/intechopen.102350.

(27) Avellan, R.; Sarrazin, M.; Spilling, C. D.; Crauste, C.; Canaan, S.; Cavalier, J.-F., Chapter 11 - Deciphering the physiological role of serine enzymes involved in mycobacterial lipid metabolism using activity-based protein profiling. In *Biology of Mycobacterial Lipids*, Fatima, Z.; Canaan, S., Eds. Academic Press: 2022; pp 235-251. DOI: https://doi.org/10.1016/B978-0-323-91948-7.00001-4.

(28) Delorme, V.; Diomandé, S. V.; Dedieu, L.; Cavalier, J.-F.; Carrière, F.; Kremer, L.; Leclaire, J.; Fotiadu, F.; Canaan, S., M*m*PPOX Inhibits *Mycobacterium tuberculosis* Lipolytic Enzymes Belonging to the Hormone-Sensitive Lipase Family and Alters Mycobacterial Growth. *PLoS ONE* **2012**, *7* (9), e46493.

(29) Point, V.; Malla, R. K.; Diomande, S.; Martin, B. P.; Delorme, V.; Carriere, F.; Canaan, S.; Rath, N. P.; Spilling, C. D.; Cavalier, J.-F., Synthesis and kinetic evaluation of Cyclophostin and Cyclipostins phosphonate analogs as selective and potent inhibitors of microbial lipases. *J Med Chem* **2012**, *55* (22), 10204-10219.

(30) Madani, A.; Mallick, I.; Guy, A.; Crauste, C.; Durand, T.; Fourquet, P.; Audebert, S.; Camoin, L.; Canaan, S.; Cavalier, J. F., Dissecting the antibacterial activity of oxadiazolone-core derivatives against *Mycobacterium abscessus*. *PLoS One* **2020**, *15* (9), e0238178.

(31) Madani, A.; Ridenour, J. N.; Martin, B. P.; Paudel, R. R.; Abdul Basir, A.; Le Moigne, V.; Herrmann, J. L.; Audebert, S.; Camoin, L.; Kremer, L.; Spilling, C. D.; Canaan, S.; Cavalier, J. F.,

Cyclipostins and Cyclophostin Analogues as Multitarget Inhibitors That Impair Growth of *Mycobacterium abscessus*. *ACS Infect Dis* **2019**, *5* (9), 1597-1608.

(32) Nguyen, P. C.; Delorme, V.; Benarouche, A.; Guy, A.; Landry, V.; Audebert, S.; Pophillat, M.; Camoin, L.; Crauste, C.; Galano, J. M.; Durand, T.; Brodin, P.; Canaan, S.; Cavalier, J. F., Oxadiazolone derivatives, new promising multi-target inhibitors against *M. tuberculosis*. *Bioorg Chem* **2018**, *81*, 414-424.

(33) Nguyen, P. C.; Delorme, V.; Bénarouche, A.; Martin, B. P.; Paudel, R.; Gnawali, G. R.; Madani, A.; Puppo, R.; Landry, V.; Kremer, L.; Brodin, P.; Spilling, C. D.; Cavalier, J.-F.; Canaan, S., Cyclipostins and Cyclophostin analogs as promising compounds in the fight against tuberculosis. *Sci Rep* **2017**, *7* (1), 11751.

(34) Nguyen, P. C.; Madani, A.; Santucci, P.; Martin, B. P.; Paudel, R. R.; Delattre, S.; Herrmann, J.-L.; Spilling, C. D.; Kremer, L.; Canaan, S.; Cavalier, J.-F., Cyclophostin and Cyclipostins analogs, new promising molecules to treat mycobacterial-related diseases. *Int J Antimicrob Agents* **2018**, *51*, 651-654.

(35) Sarrazin, M.; Martin, B. P.; Avellan, R.; Gnawali, G. R.; Poncin, I.; Le Guenno, H.; Spilling, C. D.; Cavalier, J. F.; Canaan, S., Synthesis and Biological Characterization of Fluorescent Cyclipostins and Cyclophostin Analogues: New Insights for the Diagnosis of Mycobacterial-Related Diseases. *ACS Infect Dis* **2022**, *8* (12), 2564-2578.

(36) Babin, B. M.; Keller, L. J.; Pinto, Y.; Li, V. L.; Eneim, A. S.; Vance, S. E.; Terrell, S. M.; Bhatt, A. S.; Long, J. Z.; Bogyo, M., Identification of covalent inhibitors that disrupt M. tuberculosis growth by targeting multiple serine hydrolases involved in lipid metabolism. *Cell Chem Biol* **2022**, *29* (5), 897-909 e7.

(37) Lehmann, J.; Cheng, T. Y.; Aggarwal, A.; Park, A. S.; Zeiler, E.; Raju, R. M.; Akopian, T.; Kandror, O.; Sacchettini, J. C.; Moody, D. B.; Rubin, E. J.; Sieber, S. A., An Antibacterial beta-Lactone Kills *Mycobacterium tuberculosis* by Disrupting Mycolic Acid Biosynthesis. *Angew Chem Int Ed Engl.* **2018**, *57* (1), 348-353.

(38) Li, M.; Patel, H. V.; Cognetta, A. B., 3rd; Smith, T. C., 2nd; Mallick, I.; Cavalier, J. F.; Previti, M. L.; Canaan, S.; Aldridge, B. B.; Cravatt, B. F.; Seeliger, J. C., Identification of cell wall synthesis inhibitors active against Mycobacterium tuberculosis by competitive activity-based protein profiling. *Cell Chem Biol* **2022**, *29* (5), 883-896 e5.

(39) Ortega, C.; Anderson, L. N.; Frando, A.; Sadler, N. C.; Brown, R. W.; Smith, R. D.; Wright, A. T.; Grundner, C., Systematic Survey of Serine Hydrolase Activity in Mycobacterium tuberculosis Defines Changes Associated with Persistence. *Cell Chem Biol* **2016**, *23* (2), 290-298.

(40) Ravindran, M. S.; Rao, S. P.; Cheng, X.; Shukla, A.; Cazenave-Gassiot, A.; Yao, S. Q.; Wenk, M. R., Targeting lipid esterases in mycobacteria grown under different physiological conditions using activity-based profiling with tetrahydrolipstatin (THL). *Mol Cell Proteomics* **2014**, *13* (2), 435-48.

(41) Tallman, K. R.; Levine, S. R.; Beatty, K. E., Small Molecule Probes Reveal Esterases with Persistent Activity in Dormant and Reactivating Mycobacterium tuberculosis. *ACS Infect. Dis.* **2016**, *2*, 936-944.

(42) Bakker, A. T.; Kotsogianni, I.; Mirenda, L.; Straub, V. M.; Avalos, M.; van den Berg, R.; Florea, B. I.; van Wezel, G. P.; Janssen, A. P. A.; Martin, N. I.; van der Stelt, M., Chemical Proteomics Reveals Antibiotic Targets of Oxadiazolones in MRSA. *J Am Chem Soc* **2023**, *145* (2), 1136-1143.

(43) Jo, J.; Upadhyay, T.; Woods, E. C.; Park, K. W.; Pedowitz, N. J.; Jaworek-Korjakowska, J.; Wang, S.; Valdez, T. A.; Fellner, M.; Bogyo, M., Development of Oxadiazolone Activity-Based Probes Targeting FphE for Specific Detection of Staphylococcus aureus Infections. *J Am Chem Soc* **2024**, *146* (10), 6880-6892.

(44) Santucci, P.; Point, V.; Poncin, I.; Guy, A.; Crauste, C.; Serveau-Avesque, C.; Galano, J. M.; Spilling, C. D.; Cavalier, J. F.; Canaan, S., LipG a bifunctional phospholipase/thioesterase involved in mycobacterial envelope remodeling. *Biosci Rep* **2018**, *38* (6), BSR20181953.

(45) Viljoen, A.; Richard, M.; Nguyen, P. C.; Fourquet, P.; Camoin, L.; Paudal, R. R.; Gnawali, G. R.; Spilling, C. D.; Cavalier, J.-F.; Canaan, S.; Blaise, M.; Kremer, L., Cyclipostins and Cyclophostin analogs inhibit the antigen 85C from *Mycobacterium tuberculosis* both *in vitro* and *in vivo*. *J. Biol. Chem.* **2018**, *293* (8), 2755–2769.

(46) Nguyen, P. C.; Nguyen, V. S.; Martin, B. P.; Fourquet, P.; Camoin, L.; Spilling, C. D.; Cavalier, J.-F.; Cambillau, C.; Canaan, S., Biochemical and structural characterization of TesA, a major thioesterase required for outer-envelope lipid biosynthesis in *M. tuberculosis*. *J Mol Biol.* **2018**, *430* (24), 5120-5136.

(47) Barelier, S.; Avellan, R.; Gnawali, G. R.; Fourquet, P.; Roig-Zamboni, V.; Poncin, I.; Point, V.; Bourne, Y.; Audebert, S.; Camoin, L.; Spilling, C. D.; Canaan, S.; Cavalier, J. F.; Sulzenbacher, G., Direct capture, inhibition and crystal structure of HsaD (Rv3569c) from *M. tuberculosis*. *FEBS J* **2023**, *290* (6), 1563-1582.

(48) Lehmann, J.; Vomacka, J.; Esser, K.; Nodwell, M.; Kolbe, K.; Ramer, P.; Protzer, U.; Reiling, N.; Sieber, S. A., Human lysosomal acid lipase inhibitor lalistat impairs *Mycobacterium tuberculosis* growth by targeting bacterial hydrolases. *MedChemComm* **2016**, *7*, 1797-1801.

(49) Haldar, S.; Chattopadhyay, A., Application of NBD-labeled lipids in membrane and cell biology. In *Fluorescent methods to study biological membranes*, Mély, Y.; Duportail, G., Eds. Springer Berlin Heidelberg, 2013; pp 37-50.

(50) Point, V.; Bénarouche, A.; Zarillo, J.; Guy, A.; Magnez, R.; Fonseca, L.; Raux, B.; Leclaire, J.; Buono, G.; Fotiadu, F.; Durand, T.; Carrière, F.; Vaysse, C.; Couëdelo, L.; Cavalier, J.-F., Slowing down fat digestion and absorption by an oxadiazolone inhibitor targeting selectively gastric lipolysis. *Eur J Med Chem.* **2016**, *123* (8), 834-848.

(51) Palomino, J. C.; Martin, A.; Camacho, M.; Guerra, H.; Swings, J.; Portaels, F., Resazurin microtiter assay plate: simple and inexpensive method for detection of drug resistance in *Mycobacterium tuberculosis*. *Antimicrob Agents Chemother* **2002**, *46* (8), 2720-2722.

(52) Li, Q.; Lau, A.; Morris, T. J.; Guo, L.; Fordyce, C. B.; Stanley, E. F., A syntaxin 1, Galpha(o), and N-type calcium channel complex at a presynaptic nerve terminal: analysis by quantitative immunocolocalization. *J Neurosci* **2004**, *24* (16), 4070-81.

(53) Bolte, S.; Cordelieres, F. P., A guided tour into subcellular colocalization analysis in light microscopy. *J Microsc* **2006**, *224* (Pt 3), 213-32.

(54) Costes, S. V.; Daelemans, D.; Cho, E. H.; Dobbin, Z.; Pavlakis, G.; Lockett, S., Automatic and quantitative measurement of protein-protein colocalization in live cells. *Biophys J* **2004**, *86* (6), 3993-4003.

(55) Dhouib, R.; Ducret, A.; Hubert, P.; Carriere, F.; Dukan, S.; Canaan, S., Watching intracellular lipolysis in mycobacteria using time lapse fluorescence microscopy. *Biochim Biophys Acta* **2011**, *1811* (4), 234-241.

(56) Goins, C. M.; Sudasinghe, T. D.; Liu, X.; Wang, Y.; O'Doherty, G. A.; Ronning, D. R., Characterization of Tetrahydrolipstatin and Stereoderivatives on the Inhibition of Essential *Mycobacterium tuberculosis* Lipid Esterases. *Biochemistry* **2018**, *57* (16), 2383-2393.

(57) Rens, C.; Laval, F.; Daffe, M.; Denis, O.; Frita, R.; Baulard, A.; Wattiez, R.; Lefevre, P.; Fontaine, V., Effects of lipid-lowering drugs on vancomycin susceptibility of mycobacteria. *Antimicrob Agents Chemother.* **2016**, *60* (10), 6193-6199.

(58) Dargham, T.; Aguilera-Correa, J. J.; Avellan, R.; Mallick, I.; Celik, L.; Santucci, P.; Brasseur, G.; Poncin, I.; Point, V.; Audebert, S.; Camoin, L.; Daher, W.; Cavalier, J.-F.; Kremer, L.; Canaan, S., A proteomic and functional view of intrabacterial lipid inclusion biogenesis in mycobacteria. *mBio* **2025**, e0147524.

(59) Dubois, V.; Pawlik, A.; Bories, A.; Le Moigne, V.; Sismeiro, O.; Legendre, R.; Varet, H.; Rodriguez-Ordonez, M. D. P.; Gaillard, J. L.; Coppee, J. Y.; Brosch, R.; Herrmann, J. L.; Girard-Misguich, F., *Mycobacterium abscessus* virulence traits unraveled by transcriptomic profiling in amoeba and macrophages. *PLoS Pathog* **2019**, *15* (11), e1008069.

(60) Trivedi, O. A.; Arora, P.; Sridharan, V.; Tickoo, R.; Mohanty, D.; Gokhale, R. S., Enzymic activation and transfer of fatty acids as acyl-adenylates in mycobacteria. *Nature* **2004**, *428* (6981), 441-5.

(61) Richard, M.; Gutierrez, A. V.; Viljoen, A.; Rodriguez-Rincon, D.; Roquet-Baneres, F.; Blaise, M.; Everall, I.; Parkhill, J.; Floto, R. A.; Kremer, L., Mutations in the MAB_2299c TetR Regulator Confer Cross-Resistance to Clofazimine and Bedaquiline in Mycobacterium abscessus. *Antimicrob Agents Chemother* **2019**, *63* (1), 10.1128/aac.01316-18.

(62) Rifat, D.; Chen, L.; Kreiswirth, B. N.; Nuermberger, E. L., Genome-Wide Essentiality Analysis of Mycobacterium abscessus by Saturated Transposon Mutagenesis and Deep Sequencing. *mBio* **2021**, *12* (3), e0104921.

(63) Daniel, J.; Deb, C.; Dubey, V. S.; Sirakova, T. D.; Abomoelak, B.; Morbidoni, H. R.; Kolattukudy, P. E., Induction of a novel class of diacylglycerol acyltransferases and triacylglycerol accumulation in *Mycobacterium tuberculosis* as it goes into a dormancy-like state in culture. *J Bacteriol* **2004**, *186* (15), 5017-30.

(64) Sirakova, T. D.; Dubey, V. S.; Deb, C.; Daniel, J.; Korotkova, T. A.; Abomoelak, B.; Kolattukudy, P. E., Identification of a diacylglycerol acyltransferase gene involved in accumulation of triacylglycerol in *Mycobacterium tuberculosis* under stress. *Microbiology* **2006**, *152* (Pt 9), 2717-2725.

(65) Gago, G.; Arabolaza, A.; Diacovich, L.; Gramajo, H., Components and Key Regulatory Steps of Lipid Biosynthesis in Actinomycetes. In *Biogenesis of Fatty Acids, Lipids and Membranes*, Geiger, O., Ed. Springer International Publishing: Cham, 2019; pp 409-433. DOI: https://doi.org/10.1007/978-3-319-50430-8_65.

(66) Aguilar-Ayala, D. A.; Tilleman, L.; Van Nieuwerburgh, F.; Deforce, D.; Palomino, J. C.; Vandamme, P.; Gonzalez, Y. M. J. A.; Martin, A., The transcriptome of *Mycobacterium tuberculosis* in a lipid-rich dormancy model through RNAseq analysis. *Sci Rep* **2017**, *7* (1), 17665.

(67) Mekonnen, D.; Derbie, A.; Mihret, A.; Yimer, S. A.; Tonjum, T.; Gelaw, B.; Nibret, E.; Munshae, A.; Waddell, S. J.; Aseffa, A., Lipid droplets and the transcriptome of *Mycobacterium tuberculosis* from direct sputa: a literature review. *Lipids Health Dis* **2021**, *20* (1), 129.

(68) Larrouy-Maumus, G.; Biswas, T.; Hunt, D. M.; Kelly, G.; Tsodikov, O. V.; de Carvalho, L. P., Discovery of a glycerol 3-phosphate phosphatase reveals glycerophospholipid polar head recycling in *Mycobacterium tuberculosis*. *Proc Natl Acad Sci U S A* **2013**, *110* (28), 11320-5.

(69) Crotta Asis, A.; Savoretti, F.; Cabruja, M.; Gramajo, H.; Gago, G., Characterization of key enzymes involved in triacylglycerol biosynthesis in mycobacteria. *Sci Rep* **2021**, *11* (1), 13257.

(70) Viljoen, A.; Gutierrez, A. V.; Dupont, C.; Ghigo, E.; Kremer, L., A Simple and Rapid Gene Disruption Strategy in *Mycobacterium abscessus*: On the Design and Application of Glycopeptidolipid Mutants. *Front Cell Infect Microbiol* **2018**, *8*, 69.

Table 1. Target proteins potentially involved in ILI accumulation after 24/48 h culture of *M. abscessus* S in MSM-NL, through CC-ABPP by LC-ESI-MS/MS analysis [a]

$HPOX_{yne}$		CyC_{31yne}		APEX2 [b]	Protein Ids	*M. tuberculosis* Ortholog	Essentiality	Protein names	Pathways
24h	48h	24h	48h						
	+		+		MAB_2891c	Rv2605c		Probable acyl-CoA thioesterase II TesB2	Biosynthesis of unsaturated fatty acids
		+			MAB_3588 *	Rv2500c		Putative acyl-CoA oxidase	Biosynthesis of unsaturated fatty acids
	+	+	+		MAB_3763 *	Rv2301 *		Probable Cutinase Cut2	Cell wall / cell processes
	+	+	+		MAB_3765 *	Rv3451 *		Probable Cutinase Cut3	Cell wall / cell processes
		+	+		MAB_3766 *	Rv3451/Rv3452 *		Probable Cutinase precursor Cut3/Cut4	Cell wall / cell processes
	+	+	+		MAB_3809c *	Rv3452 *	GA	Probable Cutinase Cut4	Cell wall / cell processes
+	+		+		MAB_3884 *	Rv2251		Possible flavoprotein	Ether lipid metabolism
	+				MAB_0598 *	Rv3559c		Short-chain dehydrogenase/reductase	Fatty acid biosynthesis
			+		MAB_0949c	Rv2589		Hypothetical aminotransferase	Fatty acid biosynthesis
	+		+	+	MAB_0952	Rv1928c		3-oxoacyl-[acyl-carrier protein] reductase	Fatty acid biosynthesis
	+		+	+	MAB_1512	Rv2524c †	ES	Probable fatty acid synthase FAS-I	Fatty acid biosynthesis
	+			+	MAB_1978c *	Rv2187 †		Probable long-chain-fatty-acid--CoA ligase FadD15	Fatty acid biosynthesis
	+		+		MAB_3592c	Rv3089		Putative medium-chain acyl-CoA ligase FadD13	Fatty acid biosynthesis
+	+		+		MAB_0612c #	Rv3546		Probable acetyl-CoA acetyltransferase FadA5	Fatty acid degradation
	+		+	+	MAB_0850 *	Rv0859		Probable acyl-CoA thiolase FadA	Fatty acid degradation
	+			+	MAB_0851 *	Rv0860		3-hydroxyacyl-CoA dehydrogenase FadB	Fatty acid degradation
	+				MAB_0900c	Rv0223c *		Bifunctional aldehyde dehydrogenase/enoyl-CoA hydratase	Fatty acid degradation
	+		+		MAB_0981c *	Rv0860		Possible enoyl-CoA hydratase/isomerase	Fatty acid degradation
+	+		+		MAB_0983c *	Rv0162c		Probable alcohol dehydrogenase, zinc-containing	Fatty acid degradation
	+				MAB_1069c	Rv0971c		Probable enoyl-CoA hydratase EchA7	Fatty acid degradation
	+		+	+	MAB_1187c *	Rv1071c		Probable enoyl-CoA hydratase	Fatty acid degradation
	+		+	+	MAB_1192c *	Rv1074c		Probable acyl-CoA thiolase FadA3	Fatty acid degradation
+	+				MAB_2085	Rv0975c	GA	Probable acyl CoA dehydrogenase	Fatty acid degradation
	+				MAB_3350 *	Rv3774		Putative enoyl-CoA hydratase/isomerase	Fatty acid degradation
	+			+	MAB_3481	Rv0231		Probable acyl-CoA dehydrogenase FadE4	Fatty acid degradation
+	+				MAB_3636c	Rv2500c		Probable acyl-CoA dehydrogenase	Fatty acid degradation
	+				MAB_3649	Rv3293		Probable aldehyde dehydrogenase	Fatty acid degradation
+	+		+	+	MAB_4437 #	Rv0244c		Probable acyl-CoA dehydrogenase FadE5	Fatty acid metabolism
			+		MAB_4780 *	Rv0636		MaoC-like dehydratase component of FAS-II	Fatty acid metabolism
	+		+	+	MAB_0255	Rv0154c †		Putative acyl-CoA dehydrogenase FadE2	Fatty acid metabolism/degradation
	+		+		MAB_0328 *	Rv0154c		Putative acyl-CoA dehydrogenase	Fatty acid metabolism/degradation
			+		MAB_0902	Rv1074c *		Probable beta-ketoadipyl-CoA thiolase	Fatty acid metabolism/degradation
	+		+	+	MAB_1463 *	Rv1323	GA	Probable acetyl-CoA acetyltransferase FadA4	Fatty acid metabolism/degradation

	+		+		MAB_2042c *****	Rv1867	GA	Acetyl-CoA C-acetyltransferase FadA	Fatty acid metabolism/degradation
	+			+	MAB_3040c *****	Rv2724c		Probable acyl-CoA dehydrogenase FadE20	Fatty acid metabolism/degradation
	+		+		MAB_3455c #	Rv3556c		Acetyl-CoA acetyltransferase FadA6	Fatty acid metabolism/degradation
	+		+		MAB_4609c	Rv0400c †		Putative acyl-CoA dehydrogenase FadE7	Fatty acid metabolism/degradation
+	+	+	+	+	MAB_0175 *****	Rv0129c *****		Antigen 85-C FbpC	Glycerolipid metabolism
			+		MAB_0177 *****	Rv3804c *****	GA	Antigen 85-A/B/C	Glycerolipid metabolism
			+		MAB_0176 *****	Rv3804c *****		Antigen 85-A	Glycerolipid metabolism
	+		+		MAB_0382 *****	Rv3696c	GD	Glycerol kinase GlpK	Glycerolipid metabolism
			+		MAB_2357	Rv1692 *****	GA	HAD superfamily hydrolase (Glycerol-1-phosphatase)	Glycerolipid metabolism
	+		+	+	MAB_3400 *****	Rv3045 *****		NADP-dependent alcohol dehydrogenase C	Glycerolipid metabolism
	+		+	+	MAB_3655c	Rv3302c	ES	Glycerol-3-phosphate dehydrogenase GlpD2	Glycerophospholipid metabolism
+	+		+		MAB_2814 *****	Rv1399c		Probable lipase LipH	Intermediary metabolism and respiration
	+		+		MAB_2818c	Rv0480c		Putative hydrolase	Intermediary metabolism and respiration
	+		+		MAB_3447c *****	Rv0220		Putative lipase/esterase LipC	Intermediary metabolism and respiration
	+		+		MAB_3810	Rv3569c *****	GA	Putative hydrolase, alpha/beta fold	Intermediary metabolism and respiration
+				+	MAB_0179	Rv3801c	ES	Probable fatty-acid-CoA ligase FadD32	Lipid biosynthesis proteins
	+		+		MAB_0425c *****	Rv3667		Acetyl-coenzyme A synthetase	Lipid biosynthesis proteins
+					MAB_1140	Rv1013		Putative polyketide synthase Pks16	Lipid biosynthesis proteins
			+		MAB_1141c *****	Rv0533c *****		3-oxoacyl-[acyl-carrier-protein] synthase 3 FabH	Lipid biosynthesis proteins
	+			+	MAB_2212	Rv1527c *****		Probable polyketide synthase Pks5	Lipid biosynthesis proteins
			+		MAB_2348	Rv1683 †		Possible long-chain acyl-CoA synthase	Lipid biosynthesis proteins
	+			+	MAB_0065c *****	Rv2724c	GA	Probable acyl-CoA dehydrogenase FadE20	Lipid metabolism
		+	+		MAB_0178	Rv3802c *****	ES	Probable Cutinase Cut6	Lipid metabolism
	+				MAB_0310c *****	Rv3720 †		Putative cyclopropane-fatty-acyl-phospholipid synthase	Lipid metabolism
	+				MAB_1188c	Rv0752c		Probable acyl-CoA dehydrogenase FadE9	Lipid metabolism
			+		MAB_2619	Rv1627c		Probable lipid-transfer protein Ltp1 (Thiolase?)	Lipid metabolism
	+		+		MAB_3860c	Rv0672 *****		Probable acyl-CoA dehydrogenase FadE8	Lipid metabolism
	+				MAB_4055c #	Rv3561		Putative acyl-CoA synthetase/ligase FadD3	Lipid metabolism
+	+	+	+		MAB_4328c	Rv0281 *****		Putative S-adenosyl-L-methionine-dependent methyltransferase	Lipid metabolism
+	+		+		MAB_4336 *****	Rv0271c		Probable acyl-CoA dehydrogenase FadE6	Lipid metabolism
		+			MAB_4587c *****	Rv3767c		Putative S-adenosyl-L-methionine-dependent methyltransferase	Lipid metabolism
	+				MAB_3234 *****	Rv2911	GA	Probable D-alanyl-D-alanine carboxypeptidase DacB	Peptidoglycan biosynthesis

a *M. tuberculosis* orthologs were retrieved using the KEGG (https://www.kegg.jp/) database and then cross-referenced with the Uniprot (https://www.uniprot.org/) and Mycobrowser (https://mycobrowser.epfl.ch/) databases for accurate **Protein names** and **Pathways**. The **Essentiality** of each *mab* gene was checked using the *Data Set S1B* (xls file) from Rifat *et al.*[62]: ES, essential gene; GA, causing growth advantage; GD, causing a growth defect. **b** Proteins previously identified using the APEX2 technology on *M. abscessus* culture in MSM-NL.[58] *****, proteins previously identified from competitive ABPP experiments on culture or total lysate of *M. abscessus*[30-31] or *M. tuberculosis*[32-33,47] with the **OX** and **CyC**. †, proteins involved in lipid metabolism and identified as part of *M. tuberculosis* ILIome.[8] #, genes predicted to encode enzymes necessary for the biochemical activation and β-oxidation of fatty acids that were up-regulated in both *M. abscessus*-infected amoebae and murine macrophages.[59]

Figure Legends

Scheme 1. General procedure for the synthesis of **(A) HPOX$_{yne}$** and **(B) HP$_{-NBD-}$OX**.

Figure 1. OX & CyC inhibitors efficiently colocalize with ILI inside bacteria and partially block TAG accumulation. **(A)** Chemical structure of the fluorescent and click-ready **OX** & **CyC** activity-based probes as well as their respective parent molecules. **(B)** Antibacterial activity of the three **OX** and **CyC** derivatives against the two variants of *M. abscessus* in broth medium, expressed as the minimal concentration leading to 50% (MIC_{50}) or 90% (MIC_{90}) of growth inhibition, as determined by the REMA assay ([a] Data from [30]; [b] Data from [35]). Values are mean of at least two independent assays performed in triplicate. IMP, imipenem; AMK, amikacin, used as control drugs. **(C)** The fluorescent **HP$_{-NBD-}$OX** and **CyC$_{31-Dansyl}$** specifically colocalized with ILI on *M. abscessus* S in nitrogen-limiting medium. Following a 24 h-culture in MSM-NL to induce ILI accumulation, lipid rich mycobacteria were harvested, re-suspended in fresh MSM-NL in presence of **HP$_{-NBD-}$OX** or **CyC$_{31-Dansyl}$** fluorescent probe for additional 24 h before chemical fixation, neutral lipids staining with Nile Red fluorescent dye, and confocal fluorescence imaging. Fluorescence controls are given in **Figure S2**. The Coloc2 plugin of ImageJ/Fiji was used to assess the colocalization between NBD or Dansyl fluorescent tag (*i.e.*, green channel) and Nile Red (*i.e.*, red channel). Summary of the correlation coefficients are shown underneath.[52-54] Micrographs are representative of 3 independent experiments with ten acquisitions per sample. **(D)** TAG accumulation is partially blocked by the click-ready **HPOX$_{yne}$** and **CyC$_{31yne}$** (Ser/Cys)-based enzyme inhibitors. Following a 24 h-culture in MSM-NL, lipid rich mycobacteria were harvested, re-suspended in fresh MSM-NL at OD_{600} of 20 and incubated with **HPOX$_{yne}$** (500 µM final concentration), **CyC$_{31yne}$** (200 µM final concentration) or DMSO for additional 24 h. Cells were collected and their lipids were extracted and analyzed by TLC, with triolein and oleic acid as standards for triacylglycerol (TAG) and free fatty acid (FFA), respectively. Each TLC plate is representative of three independent experiments. Results from densitometry are expressed as mean values ± SD of three biologically independent experiments, and reported as relative values using the TAG levels of *M. abscessus* WT in the MSM-NL as 100%. Statistical significance was assessed with one-way ANOVA followed by Tukey's multiple comparisons post-hoc test using Prism 8.0 (GraphPad, Inc): ** *p*-value <0.01; *** *p*-value <0.001; *ns*, not significant (*p*-value >0.05).

Figure 2. Click chemistry activity-based protein profiling in living *M. abscessus* in MSM-NL. **(A)** Click-chemistry activity-based protein profiling (CC-ABPP) typical workflow for the identification of proteins covalently bound to the **HPOX$_{yne}$** or **CyC$_{31yne}$** inhibitors. A 24 h or 48 h

growth phase culture of *M. abscessus* S was pre-treated with either **HPOX$_{yne}$** or **CyC$_{31yne}$** prior to cell lysis and subsequent click reaction with Azide-PEG$_3$-Desthiobiotin reporter. Samples were treated with streptavidin-agarose beads for the capture and enrichment of labeled proteins, followed by tryptic digestion. Tandem mass spectrometry analyses and subsequent differential peptides analysis allowed the identification of the target enzymes captured by the two inhibitors. **(B)** Volcano plot of the differential proteomic analysis between MSM-NL and MSM captured enzymes by **HPOX$_{yne}$** and showing the significance of two sample *t*-test (-Log(*p*-value)) *versus* fold-change (Log$_2$(LFQ normalized intensity in NSN-NL *vs*. MSM condition)) on the *y* and *x* axes, respectively. The dashed lines indicate the threshold of *p-value* ≤ 0.05 and a fold-change ≥ 1.0. Purple dots represent proteins potentially involved in mycobacterial lipid metabolism. **(C)** Venn diagrams showing the total number of the most abundant proteins differentially captured by **HPOX$_{yne}$** or **CyC$_{31yne}$**, respectively, from a 24 h or 48 h culture in MSM-NL; and the functional categories of *M. abscessus* proteins identified with the two probes, according to the functional classification system of the KEGG and Mycobrowser databases. The numbers correspond to the total number of identified proteins in each category. Proteins without functional annotation are denoted as uncharacterized proteins. **(D)** Venn diagrams showing the total number of proteins potentially involved in lipid metabolism that were differentially captured by **HPOX$_{yne}$** or **CyC$_{31yne}$** from a 24 h or 48 h culture in MSM-NL, and total merged captured enzymes from each probe (medium panel). **(E)** Venn diagram showing the total number of *M. abscessus* proteins potentially involved in lipid metabolism that were differentially captured from a 24 h or 48 h culture in MSM-NL and their corresponding functional categories.

Figure 3. **MAB_1978c (FadD15) is essential for TAG production and subsequent accumulation in the form of ILI in *M. abscessus*. (A)** TAG levels from *M. abscessus* cultures in MSM-NL. Cultures were collected after a 24 h or 48 h incubation period, lyophilized and equal weights of dry cells were used for apolar lipid extraction. TAG levels from *M. abscessus* WT, Δ*fadD15*, and its complemented strain Δ*fadD15*::C as well as the *fadD15-sf*GFP overexpressing strain were analyzed by TLC, with triolein and oleic acid as standards for TAG and FFA, respectively. Results from densitometry are expressed as mean values ± SD of three biologically independent experiments, and reported as relative values using the TAG levels of *M. abscessus* WT in the MSM-NL as 100%. Statistical significance was assessed with one-way ANOVA followed by Tukey's multiple comparisons post-hoc test using Prism 8.0 (GraphPad, Inc): * *p*-value <0.05; **** *p*-value <0.0001; *ns*, not significant (*p*-value >0.05). **(B)** ILI accumulation is strongly altered in the Δ*fadD15* mutant strain. Following a 48 h-culture in MSM or MSM-NL medium, mycobacteria were harvested, fixed with 4% paraformaldehyde, stained for neutral lipids with Nile Red fluorescent dye, and processed for confocal fluorescence imaging. Micrographs are representative of two biologically independent

experiments. Quantitative analysis of the Nile Red fluorescence signal per bacterium is shown as a violin plot and expressed as mean pixel intensity arbitrary units (a.u.). The *p*-values were calculated by using a two-tailed *t*-statistic test with Prism 8.0 (Graphpad, Inc): **** *p*-value <0.0001; *** *p*-value <0.001. **(C)** The FadD15-*sf*GFP protein specifically colocalizes with ILI in *M. abscessus*. Following a 48 h-culture in MSM-NL to induce ILI accumulation, lipid-rich mycobacteria were harvested, chemically fixed, stained with Nile Red fluorescent dye, and processed for confocal fluorescence imaging. Fluorescence controls are given in **Figures S6-S7**. **Sub-panel (a)**: large field image representative of the dataset acquired. **Sub-panel (b)**: zoom on a single bacterium to demonstrate *sf*GFP fluorescent colocalization with ILI when cultured in MSM-NL. **Sub-panel (c)**: plot of the fluorescence intensity of the *sf*GFP channel and the Nile Red channel as a function of the distance of each pixel from the yellow line depicted in **sub-panel (b)**, showing that both channels have the same superimposed fluorescence optimum, supporting colocalization. **Sub-panel (d)**: The Coloc2 plugin of ImageJ/Fiji was used to quantify the colocalization between *sf*GFP fluorescent tag (*i.e.*, green channel) and the Nile Red (*i.e.*, red channel). Summary of the correlation coefficients are shown underneath.[52-54] Micrographs are representative of three biologically independent experiments with ten acquisitions per sample.

Figure 4. **Schematic diagram of the biosynthetic pathways involved in TAG accumulation in the form of ILI in in *M. abscessus*.** This pathway provides a brief overview of the main findings and illustrates the involvement of proteins belonging to the lipid metabolism's functional category in TAG formations and storage as ILI following *M. abscessus* growth in MSM-NL.

For Table of Contents Use Only

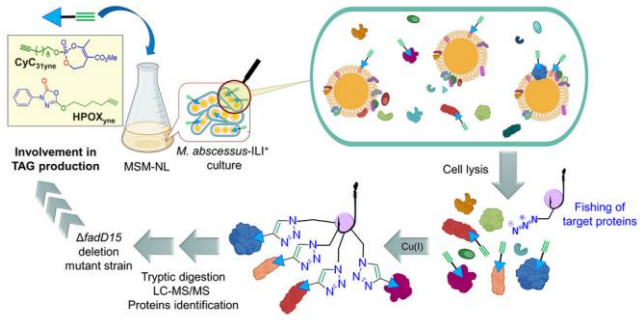

Scheme 1

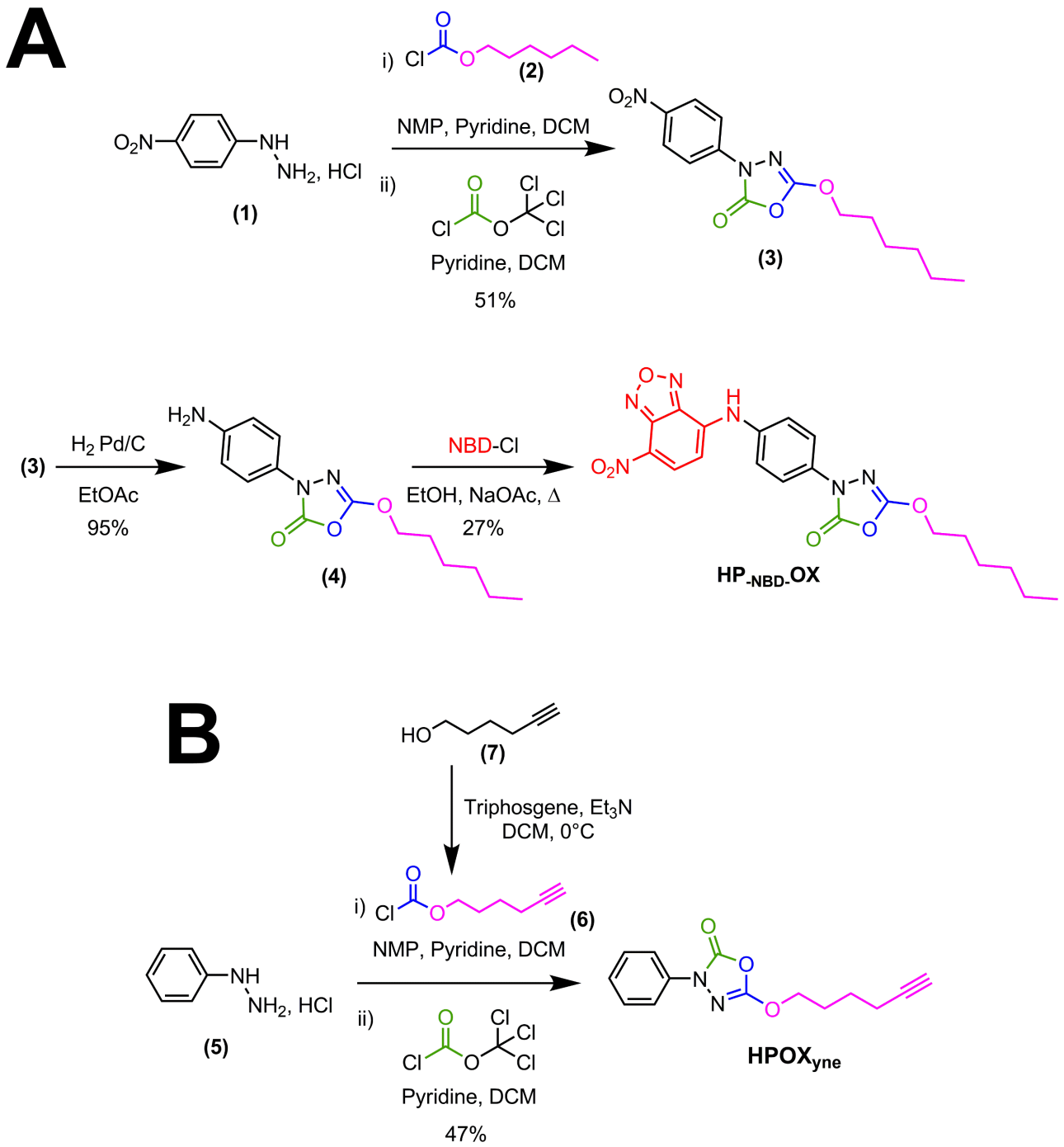
A
i) Cl
(2)
O2N
NH
NH2, HCl
(1)
NMP, Pyridine, DCM
ii)
Cl
Cl
Cl
Pyridine, DCM
51%
(3)
(3)
H2 Pd/C
EtOAc
95%
H2N
(4)
NBD-Cl
EtOH, NaOAc, Δ
27%
HP-NBD-OX
B
HO
(7)
Triphosgene, Et3N
DCM, 0°C
i) Cl
(6)
NMP, Pyridine, DCM
(5)
ii)
Pyridine, DCM
47%
HPOXyne

Figure 1

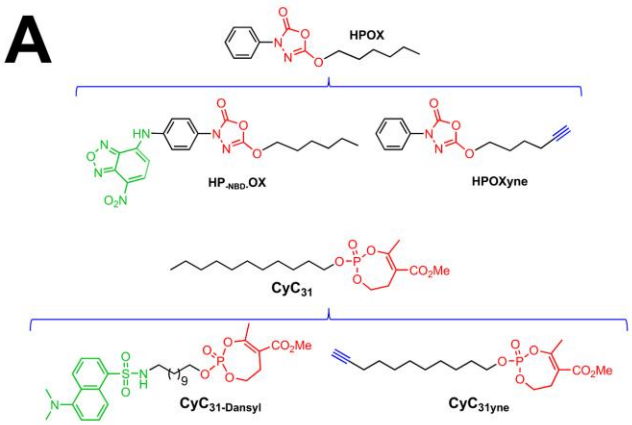

B

	MIC50 / MIC90 (μM) against *M. abscessus*	
	S variant	R variant
HPOX [a]	92.9±4.2 / 99.9±5.5	>200
$HPOX_{yne}$	90.8±1.1 / 133±3.3	>200
HP_{-NBD}-OX	66.4±2.9 / 199±7.9	>200
CyC_{31} [b]	0.56±0.05 / 1.2±0.30	6.6±0.1 / 27.1±1.6
CyC_{31yne}	0.84±0.04 / 2.1±0.10	10.3±0.35 / 18.5±1.3
$CyC_{31\text{-}Dansyl}$ [b]	1.4±0.10 / 6.1±0.39	24.1±1.10 / 63.4±2.9
AMK	3.9±0.19 / 5.8±0.20	7.4±0.26 / 10.1±0.45
IMP	4.2±0.19 / 6.3±0.26	11.9±0.63 / 29.9±1.1

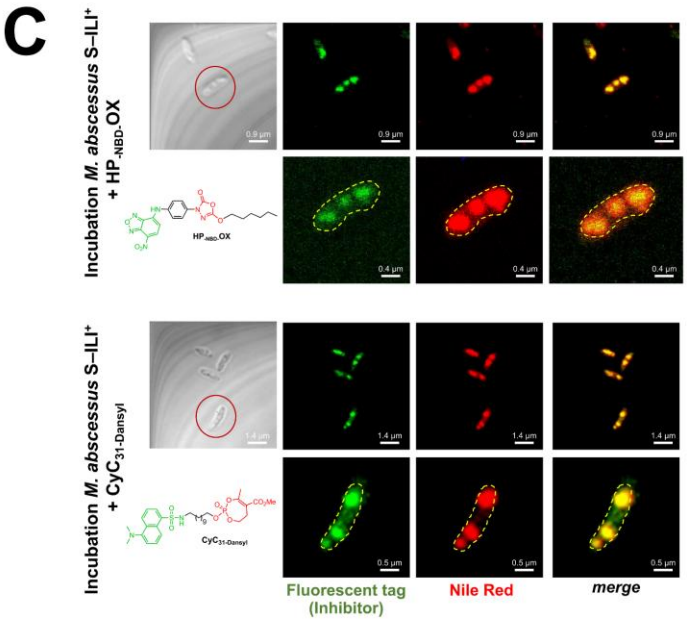

Coloc2 colocalization analysis	Dansyl	NBD
Pearson's correlation coeff. *R* value	0.808±0.020	0.788±0.028
Manders' colocalization coefficient *M1*	0.881±0.040	1
Manders' colocalization coefficient *M2*	0.845±0.043	1
Li's ICQ value	0.324±0.016	0.280±0.019
Costes *p*-Value	1	1

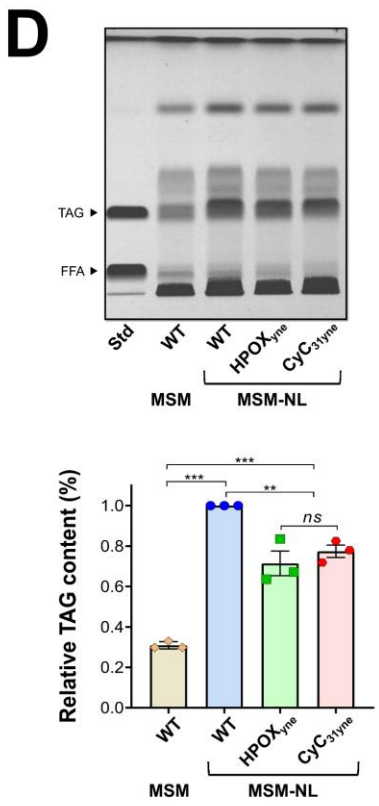

Revised Figure 2

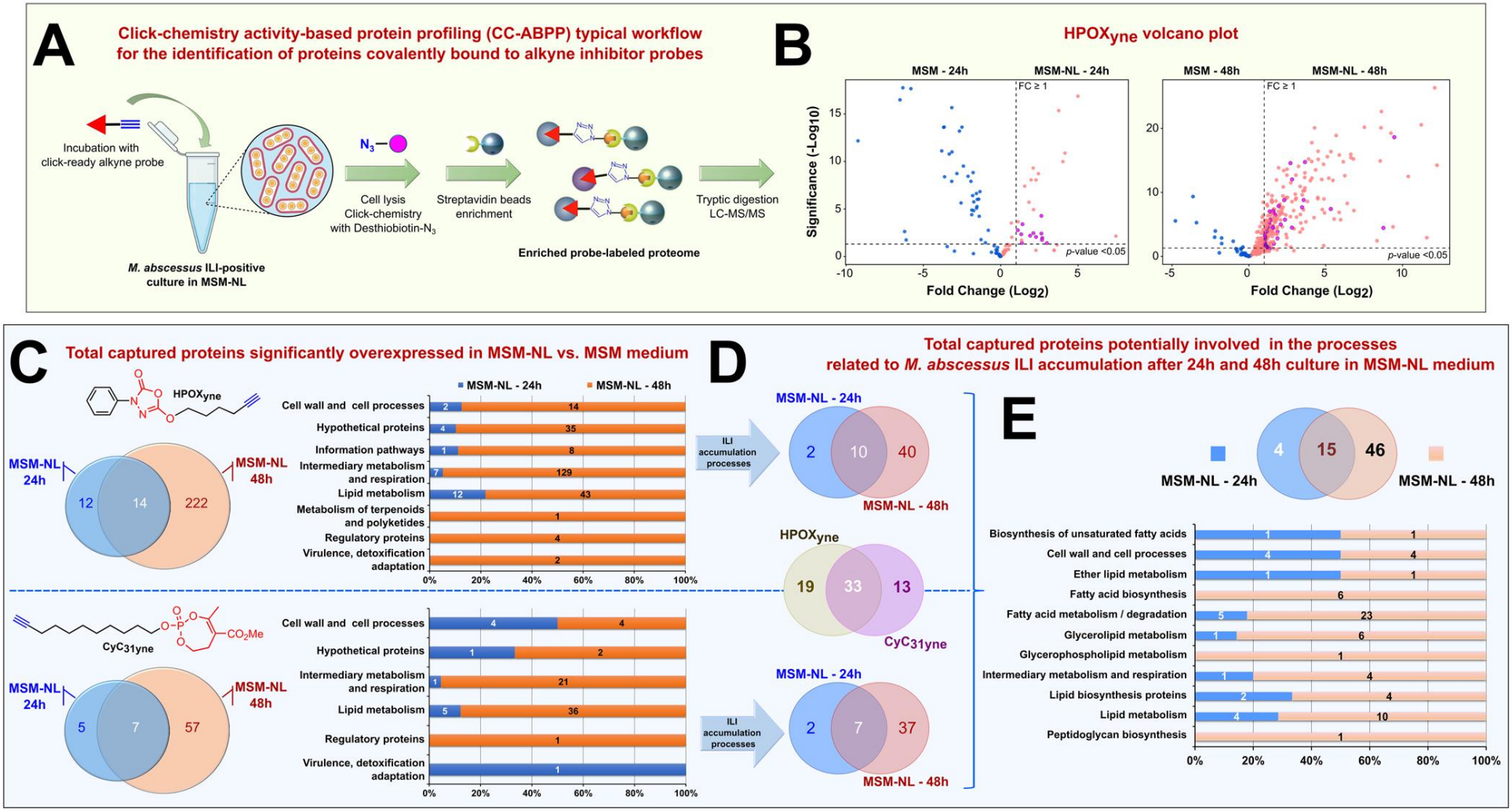

Figure 3

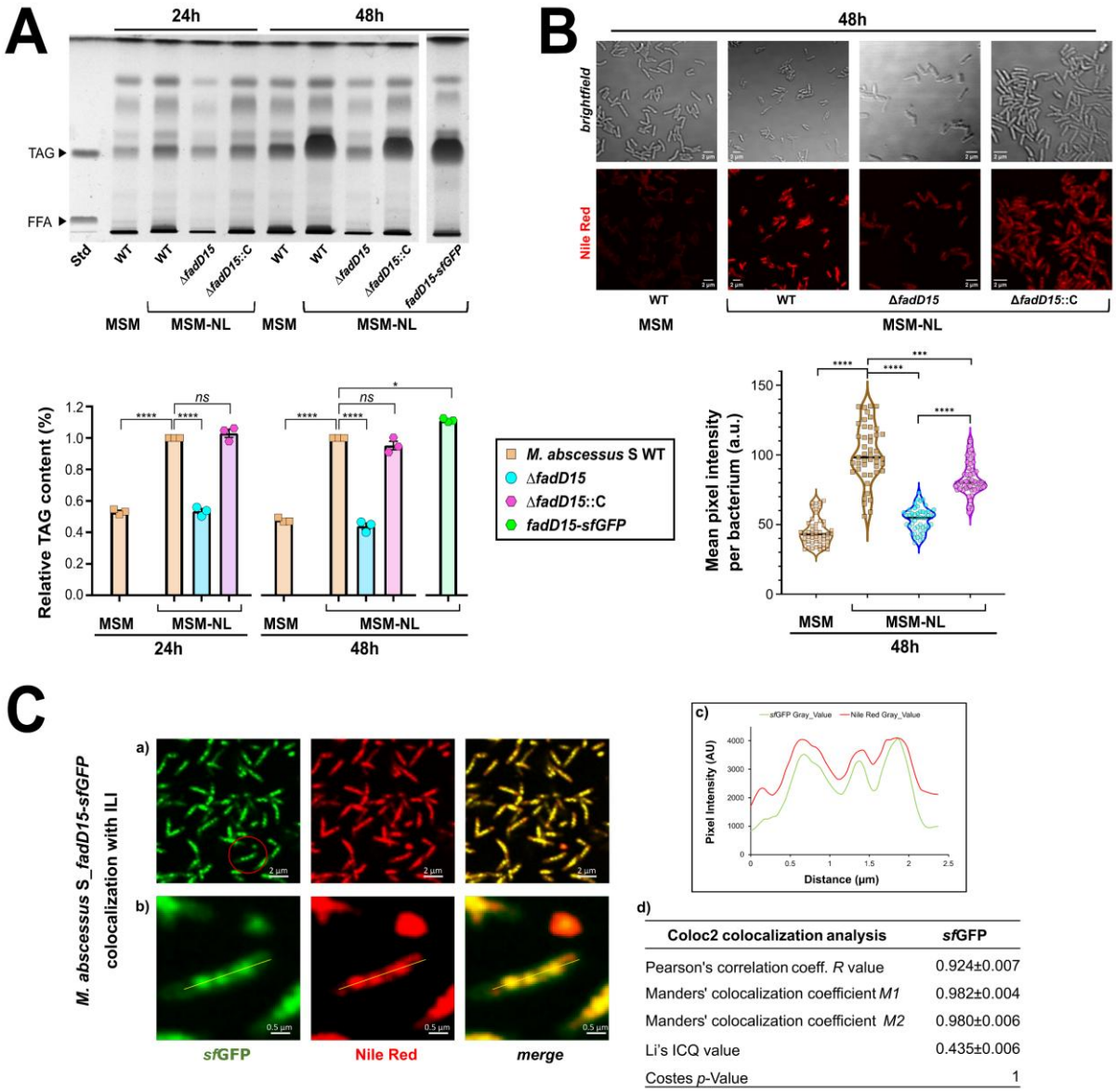

Coloc2 colocalization analysis	*sf*GFP
Pearson's correlation coeff. *R* value	0.924±0.007
Manders' colocalization coefficient *M1*	0.982±0.004
Manders' colocalization coefficient *M2*	0.980±0.006
Li's ICQ value	0.435±0.006
Costes *p*-Value	1

Figure 4

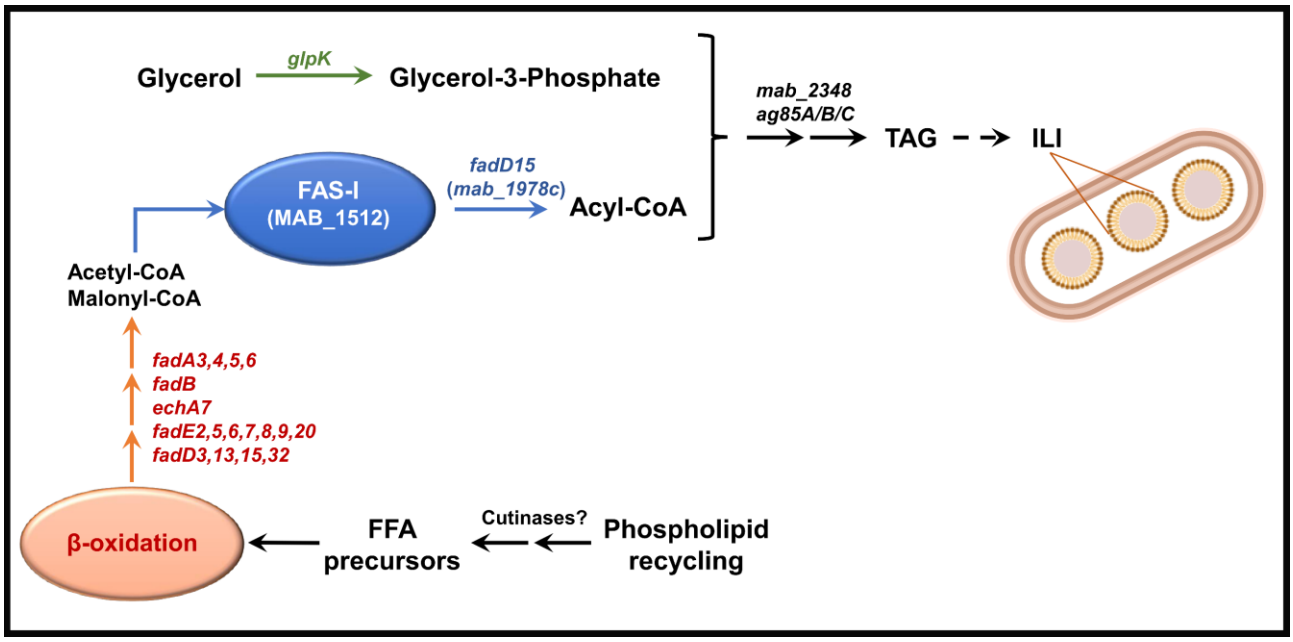
Glycerol
glpK
Glycerol-3-Phosphate
mab_2348
ag85A/B/C
TAG
ILI
FAS-I
(MAB_1512)
fadD15
(mab_1978c)
Acyl-CoA
Acetyl-CoA
Malonyl-CoA
fadA3,4,5,6
fadB
echA7
fadE2,5,6,7,8,9,20
fadD3,13,15,32
β-oxidation
FFA
precursors
Cutinases?
Phospholipid
recycling